Neutron Star Cooling

D. G. Yakovlev [1] *and C. J. Pethick* [2]

[1]Ioffe Physical Technical Institute, Politekhnicheskaya 26, 194021 St.-Petersburg, Russia, e-mail: yak@astro.ioffe.ru

[2]NORDITA, The Nordic Institute for Theoretical Physics, Blegdamsvej 17, DK–2100 Copenhagen Ø, Denmark, e-mail: pethick@nordita.dk

Abstract

Observation of cooling neutron stars can potentially provide information about the states of matter at supernuclear densities. We review physical properties important for cooling such as neutrino emission processes and superfluidity in the stellar interior, surface envelopes of light elements due to accretion of matter and strong surface magnetic fields. The neutrino processes include the modified Urca process, and the direct Urca process for nucleons and exotic states of matter such as a pion condensate, kaon condensate, or quark matter. The dependence of theoretical cooling curves on physical input and observations of thermal radiation from isolated neutron stars are described. The comparison of observation and theory leads to a unified interpretation in terms of three characteristic types of neutron stars: high-mass stars which cool primarily by some version of the direct Urca process; low-mass stars, which cool via slower processes; and medium-mass stars, which have an intermediate behavior. The related problem of thermal states of transiently accreting neutron stars with deep crustal burning of accreted matter is discussed in connection with observations of soft X-ray transients.

1 INTRODUCTION

Neutron stars are the most compact stars in the Universe. They have masses $M \sim 1.4\ M_\odot$ and radii $R \sim 10$ km, and they contain matter at supernuclear densities in their cores. Our knowledge of neutron star interiors is still uncertain and, in particular, the composition and equation of state of matter at supernuclear densities in neutron star cores cannot be predicted with confidence. Microscopic calculations are model dependent and give a range of possible equations of state (e.g., Lattimer & Prakash 2001; Haensel 2003), from stiff to soft ones, with different compositions of the inner cores (nucleons, pion or kaon condensates, hyperons, quarks).

One of the strong incentives for studying the thermal evolution of neutron stars is the promise that, by confronting observation and theory, one may learn about matter in the stellar interior. The foundation of the theory of neutron star cooling was laid by Tsuruta & Cameron (1966). The development of the theory was reviewed in the 1990s, e.g., by Pethick (1992), Page (1998a, b), Tsuruta (1998), and Yakovlev et al. (1999). The latter authors presented also a historical review covering earlier studies. Some recent results have been summarized by Yakovlev et al. (2002b, 2004a). In this paper we shall discuss the current state of the cooling theory and compare it with observations of thermal radiation

from isolated neutron stars. We shall also outline the related problem of accreting neutron stars and its application to the quiescent radiation from soft X-ray transients. We shall describe mainly results that have been obtained since the middle of 1990s. The emphasis in this review is on discussing the dependence of the cooling behavior of neutron stars on physical properties of the matter and comparing the results with observation, rather than giving a detailed account of the results of microscopic theory.

2 OBSERVATIONS

Let us begin by describing observations of thermal radiation from isolated neutron stars – cooling neutron stars which are not reheated by accretion. The detection of the thermal radiation is a complicated problem. Active processes in magnetospheres of young pulsars (with ages $t \sim 1000$ yrs) result in strong non-thermal emission which obscures the thermal radiation. Old pulsars ($t \gtrsim 10^6$) may have hot polar spots due to the pulsar activity, and the radiation from these spots may be stronger than the thermal radiation from the rest of the stellar surface, which is colder. This complicates the extraction of the thermal radiation component from the observed spectra.

  As a result of these difficulties, thermal radiation has been reliably detected only from several isolated middle-aged neutron stars ($t \sim 10^4 - 10^6$ yrs), where it appears to be an appreciable fraction of the total radiation. The main parameters of these stars (rotation period P, distance D, and surface magnetic field B) are listed in Table 1; ages t and effective surface temperatures T_s are presented in Table 2 and Fig. 1 and discussed below. The surface temperatures are $T_\mathrm{s} \sim (0.5 - 1) \times 10^6$ K. Thus, the thermal radiation is emitted mainly in soft X-rays, which can be detected by orbital X-ray observatories. The first X-ray observatories of such a type were *Einstein* (1978–1981) and *EXOSAT* (1983–1986). A very important contribution to observations of cooling neutron stars was made by the *ROSAT* observatory (1990–1998). A new era began in 1999 with the launching of *Chandra* and *XMM-Newton*, new X-ray observatories of outstanding capability. The Rayleigh-Jeans tail of the thermal emission from some isolated neutron stars has been observed in the optical with ground-based telescopes.

  To compare the observations with theory, we need mainly the neutron star effective temperatures T_s and ages t. Because neutron stars are compact, the effects of general relativity must be taken into account (see, e.g., Shapiro & Teukolsky 1983, Thorne 1977). To be specific, we shall denote the gravitational mass of the star by M and its circumferential radius by R; T_s will denote the effective temperature and $L_\gamma = 4\pi R^2 \sigma T_\mathrm{s}^4$ the thermal photon luminosity in the local reference frame of the star. Here σ is the Stefan-Boltzmann constant. The apparent (redshifted) effective temperature T_s^∞ and luminosity L_γ^∞, as detected by a distant observer, are

$$T_\mathrm{s}^\infty = T_\mathrm{s} \sqrt{1 - r_g/R} \quad \text{and} \quad L_\gamma^\infty = L_\gamma \, (1 - r_g/R), \tag{1}$$

where $r_g = 2GM/c^2 \approx 2.95 \, M/M_\odot$ km is the Schwarzschild radius. One often introduces the apparent radius $R_\infty = R/\sqrt{1 - r_g/R}$ which the observer would

see if the telescope could resolve the star. The surface temperature distribution of a magnetized star is nonuniform, and for this case we shall introduce the mean effective temperature defined by $\bar{T}_{\rm s}^4 = L_\gamma/(4\pi R^2 \sigma)$, where L_γ is the total thermal luminosity.

The values of $T_{\rm s}$ are obtained by fitting the observed spectra with theoretical models. The model spectra usually include thermal and non-thermal components. The thermal component is described (e.g., Zavlin & Pavlov 2002) either by a black-body spectrum or by a spectrum provided by a neutron star atmosphere model (with or without a magnetic field). The atmosphere models studied theoretically in greatest detail are those composed of hydrogen. The depth from which a photon emerges from a hydrogen atmosphere increases noticeably with photon energy due to the strong energy dependence of radiative opacities. Thus, more energetic photons emerge from deeper (and hotter) layers and make the spectra harder than the black-body one, for the same $T_{\rm s}$ (i.e., for the same thermal flux $\sigma T_{\rm s}^4$). The values of $T_{\rm s}$ inferred from hydrogen atmosphere models are typically about one half of those inferred using a black-body spectrum. Iron atmosphere models give spectra whose gross behavior is close to the black-body spectrum, but with spectral lines in addition. Theoretical atmosphere models are still far from perfect, especially for cool stars ($T_{\rm s}$ much below 10^6 K) and for stars with strong magnetic fields ($B \gtrsim 10^{12}$ G), because of the problems of ionization equilibrium and spectral opacities in the cool and/or strongly magnetized atmospheric plasma.

The parameters used for fitting observed spectra are: $T_{\rm s}$, R, the surface gravity g (and hence, the stellar mass M, which is completely determined by R and g), and the surface chemical composition. One can also add at least two parameters for the non-thermal radiation component (described commonly by a power-law spectrum and specified by an intensity and a power-law index). One should, in addition, specify the distance to the star and correct the theoretical spectrum for interstellar absorption, i.e., specify the column density of interstellar hydrogen. The distances and column densities can be highly uncertain. In such cases, they too are treated as free parameters. Thus, the fitting contains many parameters. Some of them are determined from the fitting procedure with large errors. To reduce the errors, one often fixes certain parameters, for instance M and R. In some cases, one needs to introduce a second thermal (black-body) radiation component characterized by its own effective surface temperature $T_{\rm s1}$ and radius R_1. One usually finds $T_{\rm s1} > T_{\rm s}$ and $R_1 < R$, in which case the second component has a natural interpretation as thermal emission from a hot spot on the stellar surface associated with the pulsar activity and not related to the thermal radiation emerging from the interior of the star. Stellar ages may also be rather uncertain. All in all, the observational data in Tables 1 and 2 represent the current state of the art. It has been a challenge to obtain them, but they are still not very precise.

Isolated (cooling) neutron stars do not constitute a homogeneous class of objects. The two youngest objects, PSR J0205+6449 and the famous Crab pulsar (PSR B0531+21), are radio pulsars in historical supernova remnants. The next two objects, RX J0822–4300 and 1E 1207.4–5209 (=J1210–5226), are radio-quiet neutron stars in the supernova remnants Puppis A and G296.5+10.0 (=PKS

Table 1: Isolated neutron stars which show thermal surface emission

Source	P [ms]	D [kpc]	$B[10^{12}$ G]	Comments
PSR J0205+6449	65	~ 3.2	3.6	PSR in SN1181
Crab	33	~ 2.5	3.8	PSR in SN1054
RX J0822–4300	75	1.9–2.5	6.8	CCO in Puppis A
1E 1207.4–5209	424	$2.1^{+1.8}_{-0.8}$	4	CCO in G296.5+10.0
Vela	89	$0.293^{+0.019}_{-0.017}$ $^{a)}$	3.4	PSR
PSR B1706–44	102	~ 2.3	3	PSR
Geminga	237	$0.159^{+0.059}_{-0.034}$ $^{a)}$	1.6	Musketeer
RX J1856.4–3754		117 ± 12 $^{a)}$		Dim object
PSR B1055–52	197	~ 0.9	1.1	Musketeer
RX J0720.4–3125	8391	~ 0.2	9.3	Dim object

$^{a)}$ parallax measured

Table 2: Observational limits on surface temperatures of isolated neutron stars

Source	t [kyr]	$T_{\rm s}^{\infty}$ [MK]	Confid.	References
PSR J0205+6449	0.82	<1.1 $^{b)}$		Slane et al. (2002)
Crab	1	<2.0 $^{b)}$	99.7%	Weisskopf et al. (2004)
RX J0822–4300	2–5	1.6–1.9 $^{a)}$	90%	Zavlin et al. (1999)
1E 1207.4–5209	$\gtrsim 7$	1.1–1.5 $^{a)}$	90%	Zavlin et al. (1998)
Vela	11–25	0.65–0.71 $^{a)}$	68%	Pavlov et al. (2001)
PSR B1706–44	~ 17	$0.82^{+0.01}_{-0.34}$ $^{a)}$	68%	McGowan et al. (2004)
Geminga	~ 340	$0.56^{+0.07}_{-0.09}$ $^{b)}$	90%	Halpern & Wang (1997)
RX J1856.4–3754	~ 500	<0.5	–	Pavlov & Zavlin (2003)
PSR B1055–52	~ 530	~ 0.7 $^{b)}$	–	Pavlov (2003)
RX J0720.4–3125	~ 1300	~ 0.5 $^{a)}$	–	Motch et al. (2003)

$^{a)}$ Inferred using a hydrogen atmosphere model
$^{b)}$ Inferred using the black-body spectrum

1209–51/52). They belong to the class of radio silent compact central objects (CCOs) in supernova remnants. CCOs have recently been reviewed by Pavlov et al. (2002b) and Pavlov & Zavlin (2003). 1E 1207.4–5209 is the first isolated neutron star found to exhibit pronounced spectral features (spectral lines) in its radiation spectrum (Sanwal et al. 2002), although the interpretation of these features seems ambiguous. The next member of the list, the Vela pulsar (PSR
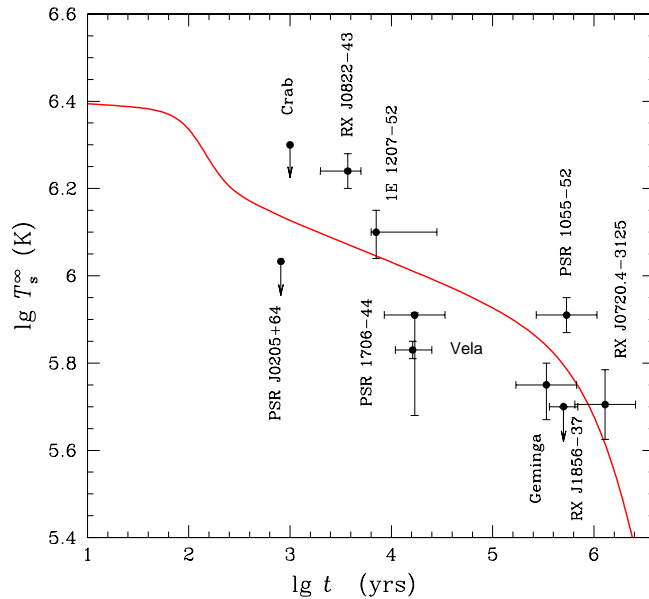
Figure 1: Observations of surface temperatures and upper bounds for several isolated neutron stars. The solid line is the basic theoretical cooling curve of a nonsuperfluid neutron star with $M = 1.3\,M_\odot$ (Sect. 5.2).

B0833–45), is almost as famous as the Crab pulsar. Among other objects, there are three neutron stars – PSR B1706–44, the Geminga pulsar (PSR B0633+1748), and PSR B1055–52 – which have been observed as radio pulsars. The properties of the radiation of two of them, Geminga and PSR B1055–52, and of another source, PSR B0656+14 (not included in our analysis as explained below), are so similar that J. Trümper has dubbed them the *three musketeers*. The other two sources in Tables 1 and 2, RX J1856.4–3754 and RX J0720.4–3125, are radio-silent, nearby, *dim*, isolated neutron stars observed in the optical band, UV and X-rays. The properties of dim objects have been reviewed by Pavlov & Zavlin (2003).

The *rotation periods* P have been measured (Table 1) for all the sources but RX J1856.4–3754 in various spectral bands (particularly, in the radio for radio pulsars and in X-rays); the measured (or estimated) time derivatives $\dot{P}$ show a familiar neutron star spindown. The *magnetic fields* B on neutron star surfaces have been determined in the standard way from P and $\dot{P}$. Numerous attempts to detect the rotation of RX J1856.4–3754 by observing periodic variations of the radiation have failed.

The *distances* D to the neutron stars in supernova remnants (PSR J0205+6449, Crab, RX J0822–4300, 1E 1207.4–5209) are the estimated distances to the remnants. The distances to the Vela pulsar (Caraveo et al. 2001, Dodson et al. 2003), Geminga (Caraveo et al. 1996), and RX J1856.4–3754 (Walter & Lattimer 2002) are reliably known from parallax measurements. In all other cases except RX J0720.4–3125, D has been determined by standard methods of radio astronomy and, consequently, the uncertainty may be large. We take the distance to RX J0720.4–3125 from Motch et al. (2003) as estimated by fitting the observed

spectrum with a neutron star atmosphere model (see below).

The *ages* (Table 2) of PSR J0205+6449 and the Crab pulsar are the well known ages of the historical supernovae. For RX J0822–43, we take the estimated age $t = 2 - 5$ kyr of the host supernova remnant (as can be deduced, e.g., from a discussion in Arendt et al. 1991), with a central value of $t = 3.7$ kyr (Winkler et al. 1988). For 1E 1207.4–5209 (as in Yakovlev et al. 2004a), we adopt the age range from the standard age of the associated supernova remnant ~ 7 kyr to a value four times longer. For Vela, we take the age interval from the standard spindown age t_c to the age estimated by Lyne et al. (1996) taking into account variations of $\dot{P}$ due to Vela's glitches. The age of RX J1856.4–3754 has been revised recently by Walter & Lattimer (2002) from the analysis of star's proper motion; the error bar is chosen to distinguish clearly the revised value from the previous one. The ages of other neutron stars are the characteristic pulsar spindown ages t_c assuming an uncertainty of a factor of 2. In particular, we take $\dot{P}$ for RX J0720.4–3125 from the recent measurements of Kaplan et al. (2002).

Finally, *effective surface temperatures* T_s^∞ in Table 2 are especially delicate. Unfortunately, no thermal radiation has been detected from the youngest objects, PSR J0205+6449 and the Crab pulsar, since their thermal emission is obscured by a strong non-thermal one. Nevertheless, upper limits on T_s^∞ for these objects have been obtained by Slane et al. (2002) and Weisskopf et al. (2004).

The surface temperatures of RX J0822–4300 and 1E 1207.4–5209 in Table 2 are taken from Zavlin et al. (1999, 1998). They have been obtained with the aid of hydrogen atmosphere models. Such results are more consistent with other data and theoretical predictions (with estimated distances to the sources, interstellar hydrogen column densities, theoretical neutron star radii) than are results based on the black-body spectrum. Recently the values of T_s^∞ for these and some other isolated neutron stars have been revised, for instance, by Pavlov et al. (2002b) and Pavlov & Zavlin (2003). The revised values are in line with the previous ones but they are presented by the authors without error bars. Accordingly, we prefer to use the previous values given with the estimated uncertainties.

The surface temperatures of the Vela pulsar and PSR B1706–44 are taken from Pavlov et al. (2001) and McGowan et al. (2004), respectively. Again they have been inferred using hydrogen atmosphere models. The surface temperature of PSR B1706–44 is much less certain because the source is more distant, but the value may be improved in the future.

The values of T_s^∞ for two musketeers – Geminga and PSR B1055–52 – are taken, respectively, from Halpern & Wang (1997) and Pavlov (2003), who obtained them with the black-body model, which seems more appropriate for these sources. The values of T_s^∞ for PSR B1055–52 have been reported without error bars, but in Fig. 1 we include, somewhat arbitrarily, 10% uncertainties in T_s^∞. Let us remark also on the third musketeer, PSR B0656+14. Recent parallax measurements for this pulsar by Brisken et al. (2003) have yielded the distance $D \approx 290$ pc, noticeably smaller than accepted before. Multiwavelength observations of the source have been reported most recently, e.g., by Zavlin & Palvov (2004). It is difficult to properly extract thermal luminosity emitted from the entire neutron star surface using either black-body or hydrogen atmosphere spectra. Thus, we do not include PSR B0656+14 in our analysis.

The surface temperature of RX J1856.4–3754 is still poorly determined. The thermal X-ray component is well fitted by the black-body spectrum, but its extrapolation to the optical band (the Rayleigh-Jeans tail) strongly underestimates the observed optical flux. It is possible that the star has a hot spot (or spots) whose radiation contaminates the emission from the rest of the surface, which is cooler. Generally, the temperature distribution over the surface may be nonuniform and the true average surface temperature is poorly determined. The nondetection of pulsed emission may be due to unfavorable orientations of radiation beams and/or due to strong gravitational lensing, which may smear out the anisotropy of the radiation. For definiteness, we have taken a model nonuniform temperature distribution suggested by Pavlov & Zavlin (2003) to fit the observations. We have calculated the appropriate average surface temperature, determined by the total photon luminosity (see above), to be $T_{\mathrm{s}}^{\infty} \approx 0.5$ MK. We propose to treat this value as an upper limit on T_{s}^{∞}. Such a limit does not contradict other estimates of T_{s}^{∞} for this source (e.g., Pons et al. 2002, Braje & Romani 2002, Burwitz et al. 2003).

The surface temperature of the last source, RX J0720.4–3125, is taken from Motch et al. (2003), who fitted the observed spectrum with a model of a hydrogen atmosphere of finite depth. The authors do not report any error bars, but we have included 20% uncertainties which we think are appropriate for this case.

The observational data are displayed in Fig. 1: they are a scatter of *sparse observational limits*. In the next sections we shall outline the theory of neutron star cooling and discuss the main issue: *what we can learn about the internal structure of neutron stars by confronting theory and observation.*

3   THEORETICAL OVERVIEW

3.1   Internal Structure

Current theories of the internal structure of neutron stars are described, e.g., by Glendenning (1996), Weber (1999), Lattimer & Prakash (2001), and Haensel (2003). A neutron star has a thin atmosphere and four internal regions, which we shall refer to as the *outer crust*, the *inner crust*, the *outer core*, and the *inner core*.

In the *outer crust* (the outer envelope), matter consists of ions (atomic nuclei) and electrons. The electrons constitute a strongly degenerate, almost ideal gas, which is relativistic at densities of order 10^6 g cm^{-3} and above. The ions form a strongly coupled Coulomb system, which is solid in most of the envelope, but which is liquid at the lowest densities. The electron Fermi energy grows with increasing ρ and, as a consequence, nuclei tend to become richer in neutrons since it is energetically favorable to convert electrons and protons into neutrons (and neutrinos) by electron capture processes. The nuclei can also undergo other transformations, such as pycnonuclear reactions, absorption and emission of neutrons. At the base of the outer crust, neutrons begin to drip out of nuclei, thereby producing a neutron gas between nuclei. This occurs at a density $\rho = \rho_{\mathrm{ND}} \approx 4 \times 10^{11}$ g cm^{-3}. The thickness of the outer crust is a few hundred meters.

In the *inner crust* (the inner envelope), matter consists of electrons, free neutrons and neutron-rich atomic nuclei (Negele & Vautherin 1973, Pethick &

Ravenhall 1995, Haensel 2003). The fraction of free neutrons increases with increasing ρ, and at the bottom of the crust (in the density range from $\approx 10^{14}$ to about $\rho_0/2$), where nuclei occupy a significant fraction of space, nuclei may be far from spherical (Lorenz et al. 1993, Pethick & Ravenhall 1995), but the detailed structure depends on the nuclear model used (Oyamatsu 1993). Here, $\rho_0 \approx 2.8 \times 10^{14}$ g cm^{-3} is the density of nuclear matter at saturation. Nuclei disappear at a density $\sim 0.5\rho_0$, and matter then becomes a uniform fluid of neutrons, protons and electrons. The thickness of the inner crust is typically about one kilometer. The equation of state throughout the crust has been calculated with reasonable accuracy, and is sufficiently well understood for the purpose of building neutron star models.

Below the inner crust lies the stellar *core*. At the lowest densities matter consists of neutrons with an admixture (several per cent by particle number) of protons, electrons, and possibly muons (the so called *npe* and *npeμ* compositions). All constituents of dense matter are strongly degenerate. The neutrons and protons, which interact via nuclear forces, constitute a strongly non-ideal liquid. For densities up to about $2\rho_0$ the equation of state and composition of matter are reasonably well constrained by nuclear physics data and theory, while at higher densities they are much less certain. We shall divide the core into an *outer core* at densities less than $\sim 2\rho_0$ and an *inner core* at higher densities. The distinction between the inner and outer cores reflects our ignorance concerning the state of matter at high density, and does not imply that matter is physically different in the two parts of the core, although it could be. In massive stars the radius of the inner core may reach several kilometers, and its central density may be as high as $(10-15)\rho_0$, while in low-mass stars the inner core may be absent since the outer core extends to the center of the star.

There are a number of possibilities for the composition of dense matter:

(1) Nucleon matter. The constituents of matter are basically the same as in the outer core.

(2) Hyperonic matter. With increasing density, the neutron and electron chemical potentials also increase, exceeding possibly thresholds for creating heavier particles such as Σ^- and Λ hyperons.

(3) Pion condensate. In dense matter, the energy of a π meson (pion) is modified by interparticle interactions and, if it becomes sufficiently low, a Bose-Einstein condensation of pion-like excitations can appear (Migdal 1971, Sawyer 1972, Scalapino 1972, Baym & Campbell 1978).

(4) Kaon condensate. The energy of a K meson (kaon) will likewise be affected by interactions, and therefore another possibility is a Bose-Einstein condensation of kaon-like excitations (Kaplan & Nelson 1986, Brown 1995) which, like real kaons, possess strangeness.

(5)Quark matter. At high densities, it is predicted that nucleons will merge to make a fluid composed of light u and d quarks and strange s quarks, and a small admixture of electrons, so-called quark matter (see Weber 1999, for a review). The appropriate degrees of freedom of such matter are then quarks and gluons, rather than nucleons and mesons. Because of the presence of s quarks, the matter is sometimes referred to as strange quark matter.

The reason that the state of matter at high density plays such an important

role in the cooling of neutron stars is that during its early life, a neutron star cools primarily by neutrino emission. Neutrino emission depends sensitively on the nature of the low-lying excitations in matter, and these are different for the different types of matter. Thus, observations of neutron star cooling may provide a way of discriminating between the various possible states of matter at high densities. The nature of matter also affects neutron star models, since the appearance of a new phase tends to soften the equation of state, and thereby alter the structure of a star.

Nuclear matter without and with hyperons have been studied experimentally in ordinary nuclei and hypernuclei. Neither boson condensation nor the deconfinement of nuclear matter have yet been discovered in nuclei in the laboratory so far. Thus, the last three models (*3*) – (*5*) are often referred to as *exotic* models of dense matter. One cannot exclude the existence of mixed phases.

The numerous theoretical equations of state may be subdivided into three classes, *soft*, *moderate* and *stiff* ones, with respect to the *compressibility* of matter. Employing different equations of state, one obtains different stellar models and, in particular, different maximum masses of a stable neutron star, from $M_{\max} \sim 1.4 \, M_\odot$ for the softest equations of state to $M_{\max} \sim (2 - 2.5) \, M_\odot$ for the stiffest ones. The appearance of a new phase tends to soften the equation of state and, consequently, the compressibility and composition are correlated. Generally speaking, very stiff equations of state are found only for nucleon matter.

Let us also mention a special hypothetical class of compact stars, called *strange* stars, which consist almost entirely of strange quark matter. According to some models, this matter extends to the very surface; such stars are referred to as *bare strange stars*. According to other models, strange stars may have a normal crust extending from the surface to the neutron-drip density. Strange stars are discussed in detail by Weber (1999).

3.2 Superfluidity

Superfluidity of nucleons in atomic nuclei is well established. Migdal (1959) predicted that neutrons in neutron stars would be superfluid. Other baryons could also be superfluid there. The superfluidity is produced by pairing (so-called Cooper pairing) of baryons due to the attractive component of their interaction, and it is present only when the temperature T of the matter falls below a critical temperature $T_{\mathrm{c}}(\rho)$, specific for a particular baryon species. An important microscopic effect is that the onset of superfluidity leads to the appearance of a gap Δ in the spectrum of elementary excitations near the Fermi surface. The pairing phenomenon is largely confined to states in the vicinity of the Fermi surface and, consequently, it has almost no effect on the equation of state, and hence on neutron star masses and radii. Superfluidity of charged particles (for instance, protons) implies that matter is superconducting.

Theory predicts that the neutrons between nuclei in the inner crust (and nucleons in nuclei) will pair in the spin *singlet state* ($^1\mathrm{S}_0$) with zero orbital angular momentum, just as electrons do in conventional metallic superconductors. However, this neutron pairing is expected to disappear in the stellar core because the neutron-neutron interaction in the singlet state becomes repulsive with increasing density (Wolf 1966). Nevertheless, a weaker interaction in the spin triplet state

(^{3}P$_2$) with unit orbital angular momentum may be still attractive in the core producing the *triplet-state pairing* of neutrons with an anisotropic gap (Hoffberg et al. 1970). (This state is a close relative of those for the superfluid phases of liquid helium 3.) Purely ^{3}P$_2$ pairing could be a simplification, because ^{3}P$_2$ channel can be superimposed with other ones, particularly, with ^{3}F$_2$. Owing to a much lower number density of protons in the core, their pairing occurs usually in the singlet state. Hyperons (Balberg & Barnea 1998) and quarks (Bailin & Love 1984) could also be superfluid. Pion and kaon condensations affect superfluidity of nucleons (e.g., Takatsuka & Tamagaki 1995, 1997).

Critical temperatures T_c of various particle species have been calculated by many authors as reviewed by Lombardo & Schulze (2001) (more references can be found in Yakovlev et al. 1999). The results are extremely sensitive to the strong interaction models and many-body theories employed. In all the cases mentioned above, microscopic theories give density dependent critical temperatures $T_c \lesssim 10^{10}$ K. All types of pairing are expected to disappear at densities well above nuclear density, where the attractive part of the strong interaction becomes ineffective.

In addition, Alford et al. (1998) proposed a new type of quark superfluidity. It consists in pairing of unlike quarks (ud, us, ds) in states which possess not only flavor but also color, in contrast to the quark pairing described above (in which a pair carries neither color nor flavor). This is referred to as *color superconductivity*. For a typical quark Fermi energy ~ 500 MeV, one may expect critical temperatures $T_c \sim 50$ MeV $\sim 5 \times 10^{11}$ K. This topic is an active area of research, and properties of stars composed of such quark matter are under investigation (see, e.g., Alford 2004 and references therein).

Because of the energy gap, superfluidity has marked effects on the heat capacity and the neutrino emissivity of dense matter. It induces also a number of macroscopic quantum phenomena (quantized neutron vortices in rotating neutron stars and quantized magnetic flux tubes in magnetized neutron-star cores, – Baym et al. 1969) but, since they are less central to the cooling of neutron stars, we do not discuss them in this review.

3.3 Neutrino Emission Processes

Neutrino emission is generated in numerous reactions in the interiors of neutron stars, as reviewed, for instance, by Pethick (1992) and Yakovlev et al. (2001a). Neutrinos carry away energy and provide efficient cooling of warm neutron stars with internal temperature $T \gtrsim (10^6 - 10^7)$ K. Neutrino reactions in the stellar crust are summarized by Yakovlev et al. (2001a). The most powerful neutrino emission is produced in the stellar core. Typical neutrino energies in nonsuperfluid stars are $\sim k_B T$, where k_B is Boltzmann's constant.

The neutrino mechanisms in the core can be subdivided into *slow* and *fast* ones. In nonsuperfluid dense matter, the emissivities of slow and fast neutrino processes can be written as

$$Q_{\text{slow}} = Q_s T_9^8, \qquad Q_{\text{fast}} = Q_f T_9^6, \qquad (2)$$

where $T_9 = T/(10^9$ K$)$, while Q_s and Q_f are slowly varying functions of ρ (whose

Table 3: Processes that provide fast neutrino emission in nucleon matter and three models of exotic matter

Model	Process		Q_{f}, erg cm^{-3} s^{-1}
Nucleon matter	$n \to pe\bar{\nu}$	$pe \to n\nu$	$10^{26} - 3 \times 10^{27}$
Pion condensate	$\widetilde{N} \to \widetilde{N}e\bar{\nu}$	$\widetilde{N}e \to \widetilde{N}\nu$	$10^{23} - 10^{26}$
Kaon condensate	$\widetilde{B} \to \widetilde{B}e\bar{\nu}$	$\widetilde{B}e \to \widetilde{B}\nu$	$10^{23} - 10^{24}$
Quark matter	$d \to ue\bar{\nu}$	$ue \to d\nu$	$10^{23} - 10^{24}$

estimates are presented in Tables 3 and 4 taken from Yakovlev & Haensel 2003 with kind permission of the authors).

Fast neutrino reactions (Table 3) have density thresholds and they are not expected to occur outside the inner core. The most powerful neutrino emission is provided by *direct Urca* [1] processes in nucleon or nucleon/hyperon matter (Lattimer et al. 1991, Prakash et al. 1992). An example of a direct Urca process is given in the first line of Table 3. It consists of a pair of reactions, the beta decay of a neutron and electron capture on a proton, whose net effect is the emission of a neutrino–antineutrino pair, the composition of matter remaining unchanged. The process can occur only if the proton concentration is sufficiently high. The reason for this is that, in degenerate matter, only particles with energies within $\sim k_{\mathrm{B}}T$ of the Fermi surface can participate in reactions, since other processes are blocked by the Pauli exclusion principle. If the proton and electron Fermi momenta are too small compared with the neutron Fermi momenta, the process is forbidden because it is impossible to satisfy conservation of momentum. Under typical conditions one finds that the ratio of the number density of protons to that of nucleons must exceed about 0.1 for the process to be allowed. Proton fractions in the outer core are estimated to be lower than this, but in the inner core they could be high enough for the process to occur. Other direct Urca processes may involve muons instead of electrons and/or hyperons instead of nucleons. In particular, a concentration of Λ hyperons of order 10^{-3} can lead to rapid neutrino emission.

Exotic phases of matter in the inner cores of massive stars would lead to fast neutrino emission by direct-Urca-like processes (see Pethick 1992, for details). Such processes are also efficient, but somewhat weaker than the nucleon direct Urca one. The leading processes of such a type in pion-condensed, kaon-condensed, and quark matter are collected in Table 3. The symbol $\widetilde{N}$ denotes a nucleon quasiparticle which, in the pion-condensed phase, is a coherent superposition of a neutron and a proton. In the kaon-condensed state, there are two types of baryonic quasiparticles, neutron-like ones which are coherent superpositions of neutrons and Σ^- hyperons, and proton-like ones which are coherent superpositions of protons, and Σ^0 and Λ hyperons (both types are denoted collectively by $\widetilde{B}$).

Slow neutrino reactions operate everywhere in the core, particularly in the

---

[1]The name *Urca* was suggested by Gamow & Schoenberg (1941), see Pethick (1992) and Yakovlev et al. (1999) for more details.

Table 4: Main processes of slow neutrino emission in nucleon matter: modified Urca and bremsstrahlung

Process			$Q_{\rm s}$, erg cm^{-3} s^{-1}
Modified Urca	$nN \to pNe\bar{\nu}$	$pNe \to nN\nu$	$10^{20} - 3 \times 10^{21}$
Bremsstrahlung	$NN \to NN\nu\bar{\nu}$		$10^{19} - 10^{20}$

outer core (and, hence, in low-mass stars). For matter consisting only of neutrons, protons and electrons, they are listed in Table 4 (where N is a nucleon, n or p). They are the modified Urca process and NN-bremsstrahlung. The modified Urca processes differ from their direct Urca counterparts by an additional spectator nucleon N required to ensure conservation of momentum and energy. There are three bremsstrahlung processes (nn, np, and pp) in npe matter. There are other modified Urca and bremsstrahlung processes in the presence of hyperons or quarks (e.g., Yakovlev et al. 2001a).

The neutrino reactions are drastically affected by baryon superfluidity as reviewed by Yakovlev et al. (1999, 2001a). When the temperature T drops much below the critical temperature $T_{\rm c}$ of a given baryon species j, the energy gap in the baryon energy spectrum makes these baryons inactive, greatly (as a rule, exponentially) suppressing all reactions involving such baryons. For instance, a strong superfluidity of protons in npe matter suppresses all Urca processes, but does not affect neutron-neutron bremsstrahlung.

While superfluidity suppresses the traditional processes, it initiates a specific neutrino process associated with *Cooper pairing of baryons* (Flowers et al. 1976). In quasiparticle language, it may be described as annihilation of two quasibaryons with the production of a neutrino pair. This process is forbidden in nonsuperfluid systems, for which the quasiparticles (the elementary excitations) are particles and holes. Two particles or two holes cannot annihilate because the total number of particles is conserved, and the annihilation of particle and a hole is forbidden for kinematical reasons. With decreasing temperature, the process begins to operate at $T = T_{\rm c}$, produces the maximum emissivity at $T \sim 0.8\,T_{\rm c}$, and becomes exponentially suppressed at $T \ll T_{\rm c}$. For realistic density profiles $T_{\rm c}(\rho)$ at T much below the maximum value of $T_{\rm c}(\rho)$, the total neutrino luminosity of the star due to this process cannot be too high: it can exceed the luminosity provided by the modified Urca process in a nonsuperfluid star at the same T by up to two orders of magnitude. The Cooper pairing neutrino process operates in the core and the inner crust.

Neutrino emissivities of many processes are model dependent, and they have not been calculated with high precision. For instance, the emissivities of the modified Urca and nucleon bremsstrahlung processes in the nonsuperfluid npe matter are usually taken from Friman & Maxwell (1979), who used the one-pion-exchange Born approximation with phenomenological corrections. Recently, neutron-neutron bremsstrahlung has been reconsidered by Hanhart et al. (2001), van Dalen et al. (2003), and Schwenk et al. (2004) using improved input for the nucleon-nucleon interactions, and their results are in reasonable agreement with

those of Friman & Maxwell (1979) (with the phenomenological corrections included). Among other recent papers, which have not been reviewed by Yakovlev et al. (2001a), let us mention the paper by Carter & Prakash (2002) who considered the renormalization of the axial weak interaction constant by in-medium effects in dense matter. Gusakov (2002) has studied the suppression of the modified Urca process by the combined action of the single-state proton pairing and the non-standard triplet-state neutron pairing with the nodes of the gap on the neutron Fermi surface. Jaikumar & Prakash (2001) have analyzed neutrino emission due to Cooper pairing of quarks.

Fortunately, cooling of neutron stars is relatively insensitive to uncertainties in the neutrino emissivity by a factor of 2–3 because the emissivity is very temperature dependent: such uncertainties are easily absorbed by small variations of the internal temperature.

3.4 Heat capacity

The major contribution to the heat capacity of a neutron star comes from the core, and it is the sum of the heat capacities of various degenerate constituents of the dense matter (the contribution of the crust is outlined, e.g, by Gnedin et al. 2001). The heat capacity per unit volume of normal (nonsuperfluid) particle species j is $c_j = m_j^* p_j k_B^2 T/(3\hbar^3)$, where p_j is the Fermi momentum, and m_j^* is the effective mass at the Fermi surface. The main contribution to the heat capacity of a nonsuperfluid core of neutrons, protons and electrons comes from neutrons, while the contribution of protons and electrons is $\sim 25\%$ and $\sim 5\%$, respectively (Page 1993). The total thermal energy of a nonsuperfluid neutron star is estimated as $U_T \sim 10^{48} T_9^2$ erg.

When T drops below a critical temperature T_c of particle species j, the heat capacity c_j first jumps up discontinuously (by a factor of 2.2–2.4) but at $T \ll T_c$ it becomes strongly suppressed (as reviewed, e.g., by Yakovlev et al. 1999). For instance, the heat capacity of an *npe* neutron star core with strongly superfluid neutrons and protons is determined by the electrons, which are not superfluid, and it is about 20 times lower than for a neutron star with a nonsuperfluid core.

4 COOLING THEORY

4.1 Basic Formalism

Neutron stars are born very hot in supernova explosions, with internal temperature $T \sim 10^{11}$ K, but gradually cool down. For about one minute following its birth, the star stays in a special *proto-neutron star* state: hot, opaque to neutrinos, and larger that an ordinary neutron star (see, e.g., Pons et al. 2001 and references therein). Later the star becomes transparent to neutrinos generated in its interior and transforms into an ordinary neutron star. We consider the cooling during the subsequent neutrino-transparent stage. The cooling is realized via two channels – by neutrino emission from the entire stellar body and by transport of heat from the internal layers to the surface resulting in the thermal emission of photons.

The internal structure of a neutron star can be regarded as temperature-independent (e.g., Shapiro & Teukolsky 1983). For a given equation of state for dense matter, one can build a family of neutron star models with different central densities ρ_c (hence, different masses and radii). Then one can simulate the cooling of any model.

The general relativistic equations of thermal evolution include the energy and flux equations obtained by Thorne (1977). For a spherically symmetric star, they are

$$\frac{e^{-\lambda-2\Phi}}{4\pi r^2}\frac{\partial}{\partial r}\left(e^{2\Phi}L_r\right) = -Q + Q_h - \frac{c_T}{e^\Phi}\frac{\partial T}{\partial t}, \quad \text{and} \tag{3}$$

$$\frac{L_r}{4\pi\kappa r^2} = e^{-\lambda-\Phi}\frac{\partial}{\partial r}\left(Te^\Phi\right), \tag{4}$$

where r is the radial coordinate (circumferential radius), Q is the neutrino emissivity, c_T is the heat capacity per unit volume, κ is the thermal conductivity, and L_r is the "local luminosity" defined as the non-neutrino heat flux transported through a sphere of radius r. For completeness, we have introduced Q_h, which represents the rate of energy production by reheating sources (if any), associated, for instance, with dissipation of rotational energy. Furthermore, $\Phi(r)$ and $\lambda(r)$ are the metric functions determined from a hydrostatic neutron-star model. The function $\Phi(r)$ specifies the gravitational redshift, while $\lambda(r)$ describes the gravitational distortion of radial scales, $e^{-\lambda} = \sqrt{1 - 2Gm(r)/c^2 r}$, where $m(r)$ is the gravitational mass enclosed within a sphere of radius r. At the stellar surface, $\Phi(R) = -\lambda(R)$.

In the outermost stellar layers (roughly, as long as electrons are nondegenerate), thermal conduction is radiative. Deeper in the crust, thermal conductivity is provided by electrons (e.g., Potekhin et al. 1997), while in the core it is produced by electrons, neutrons, and other baryons.

It is conventional (e.g., Gudmundsson et al. 1983) to separate the stellar interior ($r < R_b$) and the outer heat-blanketing envelope ($R_b \leq r \leq R$), where the boundary radius R_b corresponds to a density $\rho_b \sim 10^{10}$ g cm^{-3} (~ 100 meters under the surface). The thermal structure of the blanketing envelope is studied separately in the stationary, plane-parallel approximation to relate the surface temperature T_s (more generally, the surface thermal luminosity, L_γ) to the temperature T_b at the inner boundary of the envelope. The $T_b - T_s$ relation is used then as the boundary condition for solving Eqs. (3) and (4) at $r < R_b$.

The main goal of the cooling theory is to calculate *cooling curves*, $T_s^\infty(t)$ (or $L_\gamma^\infty(t)$), to be compared with observations. One can distinguish three main cooling stages:

(*i*) The initial *thermal relaxation stage* lasts for $t \lesssim 10$–100 yrs; the crust remains thermally decoupled from the core, and the surface temperature reflects the thermal state of the crust (Lattimer et al. 1994, Gnedin et al. 2001).

(*ii*) The *neutrino cooling stage* (neutrino luminosity $L_\nu \gg L_\gamma$) lasts for $t \lesssim 10^5$ yr; the cooling is produced by neutrino emission from the stellar interior (mainly from the core), while the surface temperature adjusts to the internal one.

(*iii*) During the final *photon cooling stage* ($L_\nu \ll L_\gamma$ $t \gtrsim 10^5$ yr) the star cools via photon emission from the surface, and the evolution of the internal temperature is governed by the radiation from the stellar surface, and hence it is sensitive to properties of the outer parts of the star.

After the thermal relaxation, the redshifted temperature $T_i(t) = T(r,t)\,\mathrm{e}^{\Phi(r)}$ becomes constant throughout the stellar interior. Then Eqs. (3) and (4) reduce to the equation of global thermal balance (Glen & Sutherland 1980),

$$C(T_i)\,\frac{\mathrm{d}T_i}{\mathrm{d}t} = -L_\nu^\infty(T_i) + L_\mathrm{h}^\infty - L_\gamma^\infty(T_\mathrm{s}), \qquad (5)$$

$$L_\nu^\infty(T_i) = \int \mathrm{d}V\, Q(T)\,\mathrm{e}^{2\Phi}, \text{ and } L_\mathrm{h}^\infty = \int \mathrm{d}V\, Q_\mathrm{h}\,\mathrm{e}^{2\Phi}, \quad C(T_i) = \int \mathrm{d}V c_T(T), \quad (6)$$

where $\mathrm{d}V = 4\pi r^2 \mathrm{e}^\lambda\,\mathrm{d}r$ is the element of proper volume, C is the total stellar heat capacity, L_ν^∞ is the total neutrino luminosity (for a distant observer), and L_h^∞ is the total reheating power.

4.2   Heat-Blanketing Envelope: $T_\mathrm{s} - T_\mathrm{b}$ Relation

An accurate T_s–T_b relation for a nonmagnetic heat-blanketing iron envelope at $T_\mathrm{s} \gtrsim 2 \times 10^5$ K was obtained by Gudmundsson et al. (1983): $T_\mathrm{b} = 1.288 \times 10^8\,(T_\mathrm{s6}^4/g_{14})^{0.455}$ K, where g_{14} is the surface gravity $g = GM\mathrm{e}^{-\Phi(R)}/R^2$ in units of 10^{14} cm s^{-2}, and $T_\mathrm{s6} = T_\mathrm{s}/10^6$ K. The thermal insulation is actually provided by a relatively thin layer of the outer part of the blanketing envelope (where the electrons are mildly degenerate); this layer becomes thinner as T_s decreases.

Potekhin et al. (1997) extended these results to lower temperatures and took into account the possible presence of a thin surface layer composed of light elements, primarily H and He, which could be the result of accretion. The thermal conductivity of the light-element plasma is higher than that of an iron plasma, thereby increasing T_s for a given T_b. The effect is determined by the total mass ΔM of the light-element envelope, and is insensitive to whether the accreted matter is H or He. Because of beta captures and pycnonuclear burning of light elements at densities $\rho \gtrsim 10^{10}$ g cm^{-3} the mass of a light-element envelope is limited to $\Delta M \lesssim 10^{-7}\,M_\odot$.

A magnetic field influences the thermal conductivity of the surface layers and, in particular, makes it anisotropic. This affects the $T_\mathrm{s} - T_\mathrm{b}$ relation (e.g., Potekhin et al. 2003 and references therein). The effects are twofold.

(1) *Classical* effects are produced by electron cyclotron motion perpendicular to the direction of the magnetic field. These effects can strongly reduce the electron thermal conductivity across the magnetic field but they do not affect the conductivity along the field. They are especially important near the magnetic equator, where the field is tangential to the surface and the heat is carried away from the stellar interior across the field lines. Such equatorial regions conduct heat less well, which lowers the local effective temperature for a given T_b.

(2) *Quantum* effects are associated with the quantization of electron motion into Landau levels. They may strongly modify the conductivities along and across the field lines. If the magnetic field is so strong that the majority of electrons occupy the lowest Landau level, the quantum effects enhance the longitudinal thermal conductivity of degenerate electrons. This effect is most pronounced near the magnetic poles, where the field is normal to the surface and heat propagates along the field lines. The quantum effects increase the local surface temperature for a given T_b.

The total photon luminosity of the star is obtained by integrating the local radiated flux over the entire stellar surface (Potekhin & Yakovlev 2001, Potekhin et al. 2003). For instance, at $T_\mathrm{s} \gtrsim 3 \times 10^5$ K the dipole magnetic field affects the luminosity if $B \gtrsim 3 \times 10^{10}$ G. As long as $B \lesssim 3 \times 10^{13}$ G, the equatorial decrease of the heat transport dominates, and the luminosity is lower than at $B = 0$. For higher B, the polar increase of the heat transport dominates, and the magnetic field increases the photon luminosity. At $B \gtrsim 10^{12}$ G the magnetic poles become much hotter than the equator. However, due to the gravitational lensing effect, the flux of thermal radiation is almost independent of the direction of observation (Page 1995, Potekhin & Yakovlev 2001).

The effects of a magnetic field are most important in the outer part of the heat-blanketing envelope and they weaken with increasing ρ. This has two consequences. *First*, in a hot neutron star ($T_\mathrm{s} \gtrsim 3 \times 10^6$ K), the most important heat-insulating layer lies deep in the blanketing envelope. As a result, the $T_\mathrm{s} - T_\mathrm{b}$ relation is weakly affected by the magnetic field, and for very high T_s it *converges to the field-free result*. Thus even a very strong field cannot change the thermal state of a hot neutron star. *Second*, the temperature distribution in the interior ($\rho > \rho_\mathrm{b}$) may be regarded as spherically symmetric. This justifies the use of the purely radial equations (3) and (4) in the internal region. In the presence of strong magnetic fields, it is reasonable to shift ρ_b to the neutron drip density, 4×10^{11} g cm^{-3} (Potekhin & Yakovlev 2001).

Recently the effects of light element envelopes and magnetic fields have been reconsidered by Potekhin et al. (2003) and Yakovlev et al. (2004b). Potekhin et al. (2003) have also studied the combined effects of light elements and magnetic fields. However, the available $T_\mathrm{s} - T_\mathrm{b}$ relations of cold ($T_\mathrm{s} \lesssim 10^5$ K) and/or strongly magnetized ($B \gtrsim 10^{13}$ G) neutron stars are still far from perfect because of the problems of calculating ionization equilibrium, the equation of state, and the thermal conductivity of cold and/or strongly magnetized plasmas.

The heat propagation time t_th through the blanketing envelope depends on many factors. For $T_\mathrm{s} \sim 10^6$ K and $\rho_\mathrm{b} \sim 10^{10}$ g cm^{-3} one has $t_\mathrm{th} \sim 1$ yr (e.g., Ushomirsky & Rutledge 2001). In a cooler star t_th is shorter due to the higher thermal conductivity.

4.3   Physical Properties that Determine Cooling

Cooling of neutron stars is affected by many factors, of which the most important are:

(a) The rate of neutrino emission from the interior of a neutron star.

(b) The heat capacity in the stellar interior.

(c) The first two items depend in turn on the composition of matter in the stellar interior, and the gross stellar structure depends on the equation of state of matter at high densities.

(d) Superfluidity of matter can have a dramatic effect on neutrino emission and the heat capacity.[2]

---

[2]In this way, as pointed out by Page & Applegate (1992), cooling neutron stars may serve as thermometers for measuring critical temperatures for nucleon superfluidity in the interiors of neutron stars.

(*e*) The thermal conductivity, especially in the heat blanketing envelope, is a crucial ingredient, because it determines the relationship between T_s and T_b. In particular, the thermal conductivity is sensitive to the presence of a light-element layer and magnetic fields in the blanketing envelope.

(*f*) Possible reheating mechanisms such as frictional dissipation of rotational energy may be especially important in cold and old neutron stars. For simplicity, we shall neglect them in cooling calculations (setting $Q_h \equiv 0$), but we shall summarize them in Sect. 5.7.

5 COOLING OF NEUTRON STARS WITH NUCLEON CORES

5.1 Physics Input

We start with the simplest composition for a neutron star core, just neutrons, protons and electrons. Illustrative cooling curves are calculated with our fully relativistic nonisothermal cooling code (Gnedin et al. 2001). In the stellar core, we use a stiff phenomenological equation of state proposed by Prakash et al. (1988) (their model I for the symmetry energy and the model of the bulk energy which gives for the compression modulus of saturated nuclear matter $K = 240$ MeV). The parameters for neutron star models with several masses are given in Table 5. Along with the values of M and R we present the central density ρ_c, the total mass of the inner and outer crusts M_{crust}, the total width of these crusts ΔR_{crust} (defined as $R - R_{core}$, where R_{core} is the radius of the crust-core interface), the mass ΔM_D and radius R_D of the central core, where the direct Urca process can occur. The most massive stable neutron star for this equation of state has $M_{max} = 1.977\,M_\odot$ and $\rho_c = 2.578 \times 10^{15}$ g cm^{-3}. For the given equation of state, the direct Urca process is allowed at densities $\rho \geq \rho_D = 7.851 \times 10^{14}$ g cm^{-3}. The mass of the star with $\rho_c = \rho_D$ is $M = M_D = 1.358\,M_\odot$.

The cooling code includes the effects of nucleon superfluidity of three types: singlet-state ($^1S_0$) pairing of free neutrons in the inner crust (with a critical temperature $T_c = T_{cns}(\rho)$); $^1S_0$ proton pairing in the core ($T_c = T_{cp}(\rho)$); and triplet-state ($^3P_2$) neutron pairing in the core ($T_c = T_{cnt}(\rho)$). The $T_c(\rho)$ dependence has been parameterized by simple equations (e.g., Yakovlev et al. 2002b); the models for $T_c(\rho)$ are qualitatively the same as those obtained in a number of microscopic calculations.

5.2 Nonsuperfluid Stellar Models

In this subsection we neglect the effects of light-element surface envelopes and surface magnetic fields. For nonsuperfluid neutron stars, we have *two* well-known cooling regimes, *slow* and *fast* cooling due to slow and fast neutrino emission (Sect. 3.3) as illustrated in Fig. 2. The left panel shows the profile of neutrino emissivity in the core at $T = 3 \times 10^8$ K with a jump by 7 orders of magnitude at the direct Urca threshold. The right panel shows cooling curves of neutron stars with several masses M: 1.1, 1.2, 1.3 $M_\odot$, M_D, $M_D + 0.01\,M_\odot$, 1.4, 1.5, 1.6, 1.7, 1.8 $M_\odot$, and M_{max}.

Table 5: Neutron star models

M ($M_\odot$)	R (km)	ρ_c (10^{14} g cm^{-3})	$M_{\rm crust}$ ($M_\odot$)	$\Delta R_{\rm crust}$ (km)	$\Delta M_{\rm D}$ ($M_\odot$)	$R_{\rm D}$ (km)
1.1	13.20	6.23	0.069	1.98	. . .	. . .
1.2	13.13	6.80	0.063	1.77	. . .	. . .
1.3	13.04	7.44	0.057	1.58	. . .	. . .
1.358^a	12.98	7.85	0.054	1.48	0.000	0.00
1.4	12.93	8.17	0.052	1.40	0.023	2.40
1.5	12.81	9.00	0.049	1.26	0.137	4.27
1.6	12.64	10.05	0.042	1.10	0.306	5.51
1.7	12.43	11.39	0.035	0.96	0.510	6.41
1.8	12.16	13.22	0.030	0.84	0.742	7.10
1.9	11.73	16.33	0.023	0.69	1.024	7.65
1.977^b	10.75	25.78	0.011	0.45	1.400	7.90

[a] Threshold configuration for the direct Urca process

[b] Maximum-mass stable neutron star
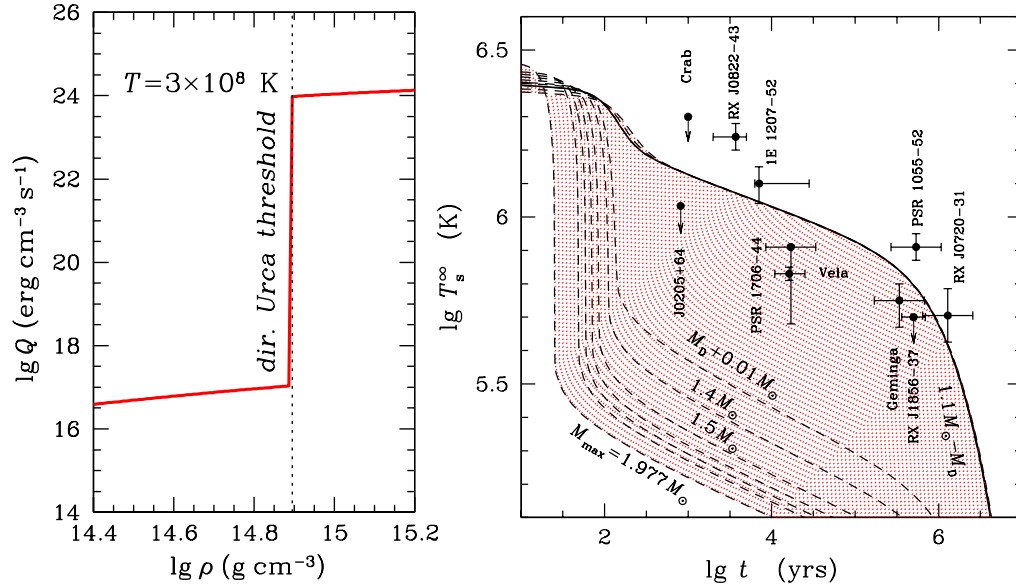
Figure 2: *Left*: Density profile of neutrino emissivity throughout the core of a nonsuperfluid neutron star at $T = 3 \times 10^8$ K. *Right*: Cooling curves for non-superfluid neutron stars of several masses compared with observations; points lying within the shaded region may formally be explained by models of cooling nonsuperfluid neutron stars with the given equation of state.

Slow cooling occurs in low-mass stars ($M < M_{\rm D}$) via neutrino emission produced mainly by the modified Urca process. The cooling curves are almost the same for all M from about $M_\odot$ to $M_{\rm D}$ (Page & Applegate 1992). The surface temperature stays high, $T_{\rm s}^\infty \gtrsim 10^6$ K, for $t \lesssim 10^5$ yrs. A simple estimate from the
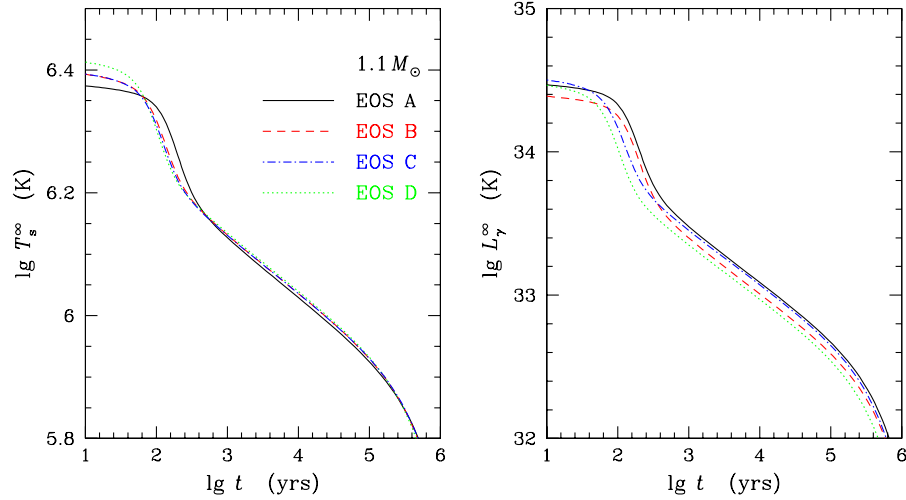
Figure 3: Surface temperatures (*left*) and photon luminosities (*right*) of non-superfluid $1.1\,M_\odot$ neutron stars for four high-density equations of state (see text).

thermal balance equation, Eq. (5), gives an approximate slow-cooling law during the neutrino cooling stage: $t_{\rm slow} \sim 1$ yr$/T_{i9}^6$ (see, e.g., Pethick 1992). The internal temperature drops to $T_i \sim 1.5 \times 10^8$ K in $t = 10^5$ yrs. These nonsuperfluid models of cooling by the modified Urca process cannot explain the observational limits of some sources, first of all, PSR J0205+6449, Vela, and PSR B1706–44 (too cold), as well as RX J0822–4300 and PSR B1055–52 (too hot). The data seem to require both slower and faster cooling.

The *fast cooling* occurs at $M - M_{\rm D} \gtrsim 0.01\,M_\odot$ via the powerful direct Urca process. The cooling curves are again not too sensitive to the stellar mass. These stars are much colder ($T_{\rm s}^\infty \lesssim 3 \times 10^5$ K for $t \sim 10^4$ yrs) than the slow-cooling ones. An estimate from Eq. (5) during the neutrino cooling stage now yields $t_{\rm fast} \sim 1$ min$/T_{i9}^4$, giving $T_i \sim 10^7$ K for $t = 200$ yrs.

The *transition* from the slow to fast cooling takes place in a very narrow range of M because of the huge difference in the emissivities of the modified and direct Urca processes, and the sharp threshold of the direct Urca process (left panel of Fig. 2). On the cooling diagram some sources (in particular, Vela, PSR B1706–44, Geminga, RX J1856.4–3754) fall exactly in this transition zone, and therefore could be explained if they had almost the same mass. This unlikely assumption can be avoided by including the effects of nucleon superfluidity (see Sect. 5.4).

Let us stress the *universality* of the cooling curves (Page & Applegate 1992). The curves for low-mass stars are insensitive not only to the values of M (as long as $M < M_{\rm D}$), but also to the equation of state at high densities. The effect is illustrated in Fig. 3, where we show the cooling of $1.1\ M_\odot$ stars, with four equations of state. Model A is our basic equation of state (Sect. 5.1), while B, C, and D are modifications of the equations of state of Prakash et al. (1988) with the simplified form of the symmetry energy suggested by Page & Applegate (1992). Specifically, models B, C, and D correspond to three values of the compression modulus of saturated nuclear matter: K=180, 240, and 120 MeV, respectively. They are examples of moderate, stiff, and soft equations of state

(yielding M_{max}=1.730, 1.942, and 1.461 $M_\odot$). Although the equations of state and the stellar models are different, the cooling curves of low-mass stars are almost the same, especially if one plots $T_{\mathrm{s}}^\infty(t)$ (left panel) rather than $L_\gamma^\infty(t)$ (right panel). This universality is easily explained from Eq. (5): the cooling rate at the neutrino cooling stage is proportional to L_ν^∞/C, the ratio of the total neutrino luminosity and heat capacity. While both L_ν^∞ and C depend on the stellar model, their ratio is almost model-independent. Thus, we have actually one universal *standard basic cooling curve* for all models with $M_\odot \lesssim M < M_{\mathrm{D}}$. This curve is plotted in Fig. 1. The cooling curves of high-mass stars are also similar (for the same reasons). For instance, the curves of maximum-mass stars with equations of state A–D are almost identical.

5.3   Effects of Magnetic Fields and Light-Element Envelopes

Now we discuss the effects of surface magnetic fields and light-element (accreted) envelopes (Sect. 4.2). We shall follow the considerations of Potekhin et al. (2003) (also see their paper for references to earlier work). Figure 4 shows slow and fast cooling of nonsuperfluid 1.3 $M_\odot$ (solid lines) and 1.5 $M_\odot$ (dashed lines) stars.

The left panel illustrates the effects of accreted envelopes in nonmagnetized stars. We present the cooling curves for some values of ΔM, the mass of relatively light elements (H, He, C, or O) in the heat-blanketing envelopes. The fraction of accreted mass $\Delta M/M$ varies from 0 (nonaccreted envelopes) to $\sim 10^{-7}$ (fully accreted envelopes; see Sect. 4.2).

During the neutrino cooling stage, the internal stellar temperature T_{b} is determined by neutrino emission, and is insensitive to the physics of the heat-blanketing envelope. The surface temperature adjusts to T_{b} according to the T_{s}–T_{b} relation. Since accreted envelopes conduct heat better than ones composed of heavier elements, the surface temperature of a star with an accreted envelope is noticeably higher. Even an amount of accreted matter as small as $\Delta M/M \sim 10^{-13}$ can appreciably change the cooling. The cooler the star, the smaller ΔM which yields the same cooling as the fully accreted blanketing envelope. The reason for this is that the greatest contribution to the difference between surface and interior temperatures occurs in a thin layer where matter is partially degenerate. The cooler the star, the closer this layer is to the surface, and the smaller the amount of accreted matter is needed to change the composition of this layer.

For $t \gtrsim 10^5$ yrs the star enters the photon cooling stage when the cooling is governed by T_{s} (Sect. 4.1). An accreted envelope leads then to faster cooling (more rapid fall of T_{s} with time). Thus, the effects of light elements on the surface temperature during the neutrino and photon cooling stages are opposite. This reversal of the effect of light elements when passing from one stage to the other has a straightforward physical explanation, and is well known.

The middle panel of Fig. 4 displays the effect of a dipolar magnetic field on the cooling of neutron stars with nonaccreted envelopes. Let us remark that in this case T_{s} refers to the average surface temperature (Sect. 2). We present the cooling curves for several strengths of the magnetic field at the poles up to $B_{\mathrm{p}} = 10^{16}$ G. The cooling curves of nonmagnetic neutron stars are shown as thick lines. For simplicity, the magnetic field is assumed to be independent of time.
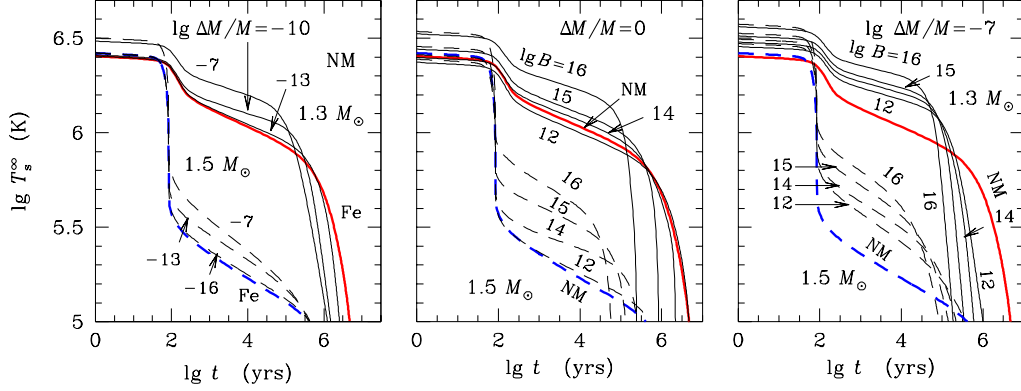
Figure 4: Cooling of nonsuperfluid neutron stars with $M = 1.3\,M_\odot$ (solid lines) and $1.5\,M_\odot$ (dashed lines). *Left*: nonmagnetic (NM) stars with different amounts ΔM of light elements in the blanketing envelopes; thick curves refer to nonaccreted (Fe) envelopes. *Middle*: stars with nonaccreted envelopes and dipole surface magnetic fields (the curves are labeled by $\lg B_{\mathrm{p}}$, and thick lines refer to $B = 0$). *Right*: same as in the middle panel but with a fully accreted envelope.

A magnetic field $B_{\mathrm{p}} \lesssim 10^{13}$ G makes the blanketing envelope of a warm $(1.3\,M_\odot)$ neutron star less conducting to heat (Sect. 4.2). This lowers T_{s} during the neutrino cooling stage and increases T_{s} during the photon cooling stage, producing another reversal effect. By contrast, a stronger magnetic field with $B_{\mathrm{p}} \gg 10^{13}$ G makes the blanketing envelope a better conductor of heat, which increases T_{s} during the neutrino cooling stage and lowers T_{s} during the photon cooling stage (another reversal). A field $B_{\mathrm{p}} \sim 10^{13}$ G has almost no effect on the cooling. The fast cooling of cooler magnetized $(1.5\ M_\odot)$ neutron stars is somewhat different: a magnetic field $B_{\mathrm{p}} \lesssim 10^{13}$ G has almost no effect on T_{s}, while fields $B_{\mathrm{p}} \gtrsim 10^{13}$ G affect the cooling much more than for slow-cooling neutron stars.

The right panel of Fig. 4 shows cooling curves for neutron stars with fully accreted envelopes and the same dipole magnetic fields as in the middle panel. For a star with $B_{\mathrm{p}} \lesssim 10^{15}$ G during the neutrino cooling stage, the effect of the accreted envelope is stronger than the effect of the magnetic field. For higher B_{p}, the magnetic effect dominates; the accreted envelope produces a rather weak additional rise in T_{s}.

The main outcome of these studies is that even ultrahigh magnetic fields do not change the average surface temperatures of young and warm neutron stars as much as an accreted envelope can. At the same time, strong fields induce a strongly nonuniform surface temperature distribution (see, e.g., Potekhin et al. 2003).

5.4 Proton Superfluidity and Three Types of Cooling Neutron Stars

The considerations above show that the effects of magnetic fields and accreted envelopes in nonsuperfluid neutron stars cannot reconcile theory and observation.
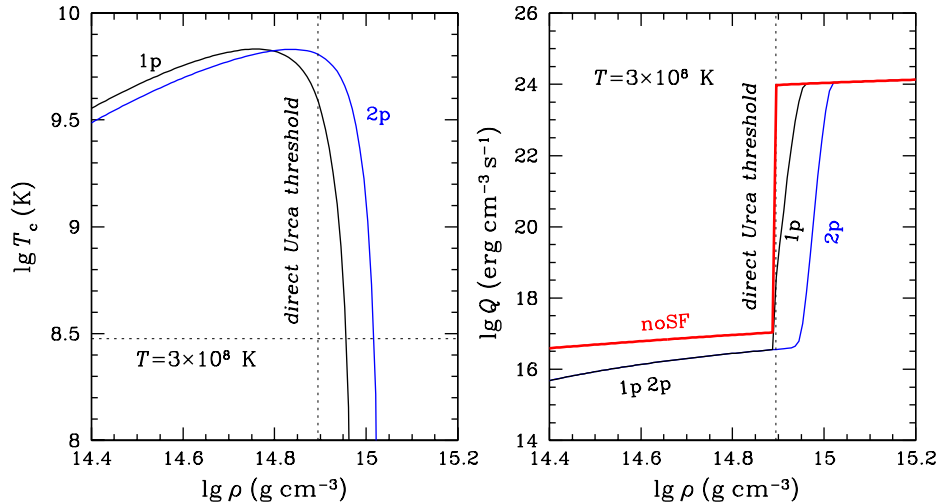
Figure 5: *Left:* Superfluid transition temperature versus density for two models (1p and 2p) for proton superfluidity in the neutron star core. *Right:* Neutrino emissivity profiles in the core at $T = 3 \times 10^8$ K for nonsuperfluid matter (noSF) and for matter with superfluid protons (models 1p or 2p).

Thus, we turn to the cooling of *superfluid* neutron stars. For simplicity, in Sects. 5.4 and 5.5 we consider nonmagnetic neutron stars without accreted envelopes.

The observations can be explained by the cooling of superfluid neutron stars assuming that *proton superfluidity is rather strong* at $\rho \lesssim \rho_D$, while the $^3P_2$ *neutron superfluidity is rather weak*. We start with the effects of proton superfluidity (Kaminker et al. 2001) and neglect neutron pairing. We take two typical models of proton superfluidity, 1p and 2p. The model critical temperatures $T_{cp}(\rho)$ are displayed in the left panel of Fig. 5. The resulting neutrino emissivity in the stellar core at $T = 3 \times 10^8$ K is shown in the right panel.

The effects of proton superfluidity are seen to be twofold. First, superfluidity reduces the neutrino emission in the outer core by strongly suppressing the modified Urca and even the direct Urca process at not too high ρ. Consequently, neutron-neutron bremsstrahlung (Table 4), which is weaker, becomes the leading neutrino emission mechanism. Second, proton superfluidity gradually dies out with increasing ρ, smoothly removing the reduction of fast neutrino emission. This broadens the direct Urca threshold, creating *a finite transition zone* at densities $\rho_s \lesssim \rho \lesssim \rho_f$ between the regions with slow neutrino emission ($\rho \lesssim \rho_s$) and rapid neutrino emission ($\rho \gtrsim \rho_f$). For model 2p, superfluidity extends deeper into the stellar core and shifts the transition zone to higher densities. The direct Urca threshold can also be broadened by the thermal effects and by magnetic fields (Baiko & Yakovlev 1999) but these effects are usually weaker than the broadening provided by superfluidity (Yakovlev et al. 2001a).

The cooling curves of neutron stars of different masses with proton superfluidity models 1p and 2p are plotted in the left and right panels of Fig. 6, respectively. We see that proton superfluidity leads to *three* characteristic types of cooling neutron stars (Kaminker et al. 2002).
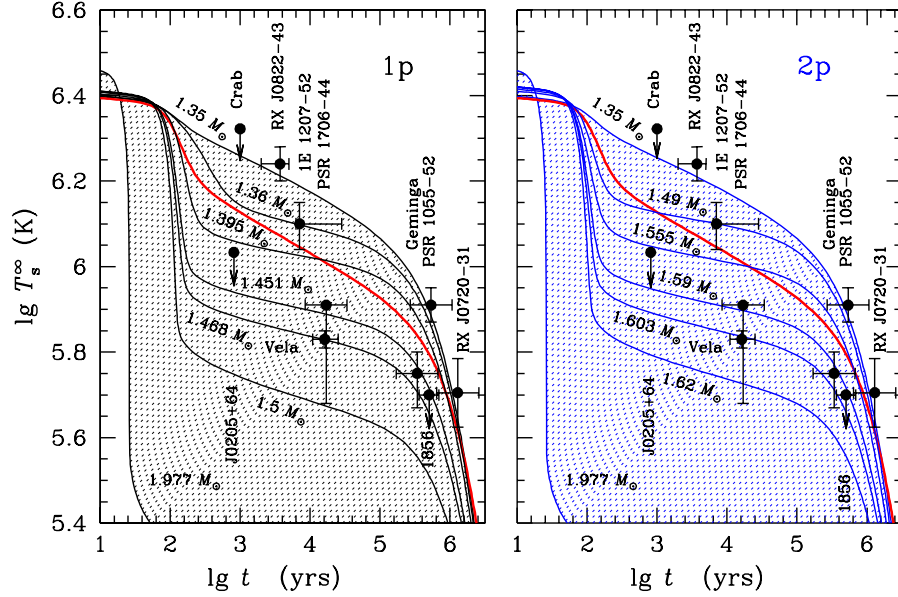
Figure 6: Cooling of neutron stars of different masses with either model 1p (*left*) or model 2p (*right*) for proton superfluidity in the cores together with observations of isolated neutron stars. Any point lying within the shaded regions can be explained by the given models for some value of the neutron star mass.

Low-mass neutron stars, with $\rho_c < \rho_s$, have weaker neutrino emission than low-mass nonsuperfluid neutron stars, and they form a class of *very slowly cooling neutron stars*. Their cooling curves are almost universal (as in Sect. 5.2): they are independent of the stellar mass, the model for proton superfluidity, and the equation of state in the stellar core. These cooling curves lie above the basic standard cooling curve, and can explain the observations of RX J0822–4300 and PSR B1055–52. Thus we can treat these two sources as low-mass neutron stars. With some reservations, RX J0720.4–3125 may also be attributed to this class (although, given the large observational uncertainties, it may belong to the class of cooler, medium-mass stars).

High-mass, rapidly cooling neutron stars, with $\rho_c \gtrsim \rho_f$, cool mainly via fast neutrino emission from the inner core. The cooling curves are again almost independent of M, equation of state and model for proton superfluidity, and they are actually the same as for high-mass nonsuperfluid stars. All observed isolated neutron stars are much warmer than these models.

Medium-mass neutron stars ($\rho_s \lesssim \rho_c \lesssim \rho_f$) show cooling which is *intermediate* between very slow and fast; it depends on M, the equation of state and proton superfluidity. Roughly, the masses of these stars range from M_D to 1.55 $M_\odot$ for the 1p superfluidity model and from 1.4 to 1.65 $M_\odot$ for the 2p superfluidity model. By varying ρ_c from ρ_s to ρ_f we obtain a family of cooling curves which fill the (shaded) space between the curves of low-mass and high-mass stars. Then we can select those curves which explain the observations and thus attribute masses to the sources. This "weighing of neutron stars" suggested by Kaminker et al. (2001) depends on a proton superfluidity model (Fig. 6) as well as on the
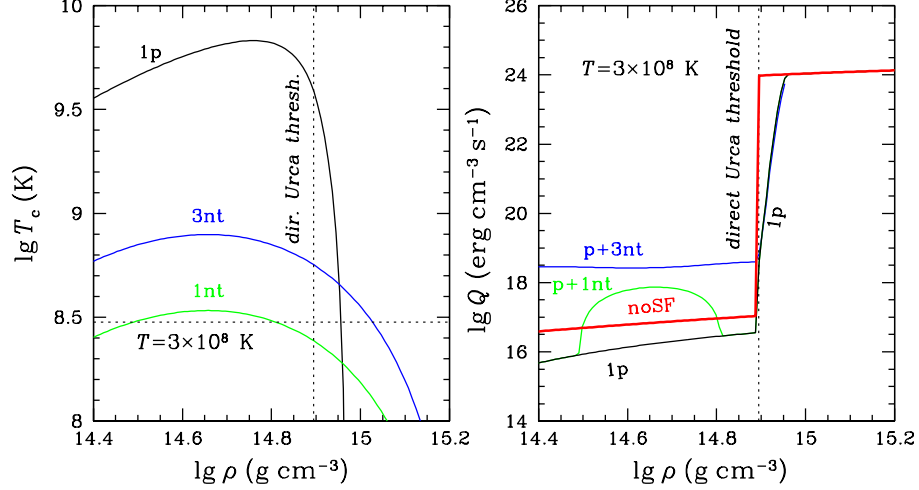
Figure 7: *Left:* Superfluid transition temperatures as a function of density for protons (model 1p) and neutrons (models 1nt and 3nt for triplet-state pairing) in the core of a neutron star. *Right:* Neutrino emissivity as a function of density at $T = 3 \times 10^8$ K in nonsuperfluid matter (noSF) and in the presence of proton superfluidity (model 1p) and neutron superfluidity (models 1nt and 3nt).

equation of state and the composition of matter in the core (see, e.g., Kaminker et al. 2002), which determine the position of the direct Urca threshold. We can treat 1E 1207–52, Vela, PSR B1706–44, Geminga, and RX J1856.4–3754 as medium-mass neutron stars.

5.5   Mild Neutron Pairing in the Core Contradicts Observation

We now investigate the effect of $^3P_2$ neutron pairing in the stellar core (e.g., Kaminker et al. 2001, 2002; Yakovlev et al. 2002a). Microscopic theories predict this pairing to be weaker than the proton one. Two models for $T_{cnt}(\rho)$ (1nt and 3nt) are presented in the left panel of Fig. 7, with maximum $T_{cnt}^{max} \approx 3.4 \times 10^8$ and 8×10^8 K, respectively. The appearance of such superfluidity induces the strong neutrino emission due to Cooper pairing of neutrons in the outer core as shown in the right panel of Fig. 7.

Theoretical cooling curves of neutron stars with model 1p for proton superfluidity and with either model 1nt or model 3nt for neutron superfluidity are shown in Fig. 8. Before the onset of neutron superfluidity the curves are the same as for models with proton superfluidity alone (Fig. 6). After the onset, cooling is strongly accelerated by neutrino emission due to the Cooper pairing of neutrons. For model 3nt, neutron superfluidity is stronger than for model 1nt and appears earlier, producing faster cooling (cf. right and left panels of Fig. 8). In any case, the fast cooling predicted by these models is in conflict with observations of many sources.

In fact any *mild* neutron superfluidity in the stellar core with a realistic $T_{cnt}(\rho)$ profile and $T_{cnt}^{max} \sim (2 \times 10^8 - 2 \times 10^9)$ K contradicts observations of at least some hotter and older objects (independently of the proton pairing) and *should be*
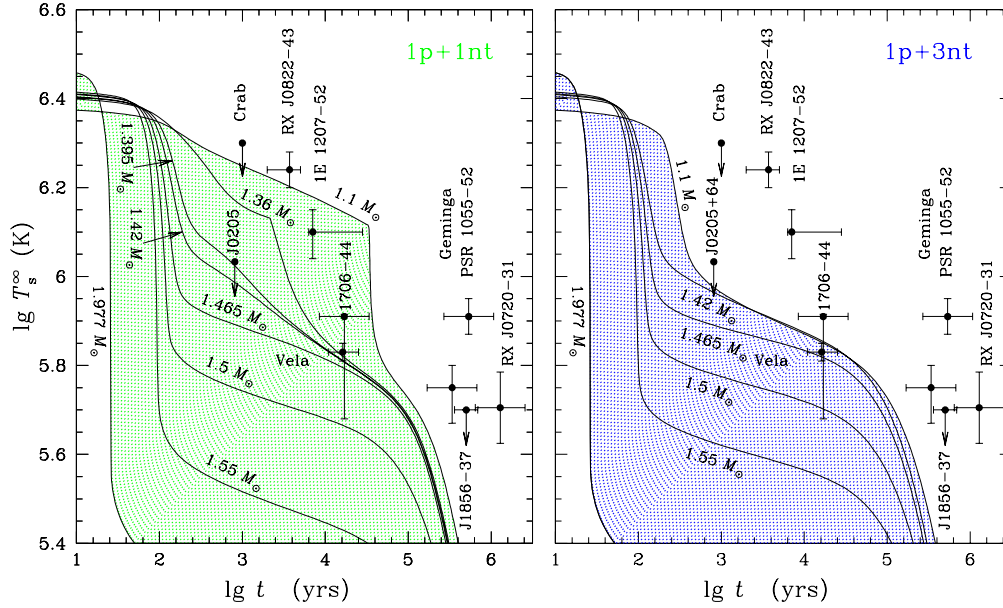
Figure 8: Cooling of neutron stars of different masses with models 1p for proton superfluidity and either 1nt (*left*) or 3nt (*right*) for neutron superfluidity in the cores together with observations of isolated neutron stars. Any point within the shaded regions may be explained by the given cooling models for some value of the stellar mass.

rejected on these grounds (Yakovlev et al. 2004a). Neutron superfluidity with a smaller $T_{\rm cnt}^{\rm max}$ would come into play only in the late stages of neutron star evolution and has no effect on the cooling of middle-aged stars. It is interesting that recent calculations by Schwenk & Friman (2004) indicate that the medium-induced one-pion-exchange interaction (acting in second order) greatly reduces triplet-state pairing of neutrons in neutron star cores. This is in line with the above conclusion that triplet-state neutron pairing should be weak.

The neutrino luminosity due to Cooper pairing of nucleons may exceed that due to the modified Urca process in normal matter by a factor of up to ~ 100. Thus, neutrino emission produced by Cooper pairing will not affect the cooling of massive neutron stars (if the direct Urca process is allowed in the inner core and superfluidity becomes weak there, unable to suppress fast neutrino emission).

In principle, the observations could be explained in the same manner as in Sect. 5.4 but assuming strong neutron superfluidity in the stellar core (instead of strong proton one) and weak proton superfluidity (instead of weak triplet-state neutron pairing). This has been shown (e.g., Yakovlev et al. 1999) in simplified cooling simulations with $T_{\rm cp}$ and $T_{\rm cnt}$ constant throughout stellar cores. However, this scenario seems less likely in view of theoretical estimates of gaps. The simultaneous presence of strong neutron and proton superfluids in the core would greatly reduce the stellar heat capacity and initiate a rapid cooling of low-mass stars at $t \gtrsim 3 \times 10^4$ yrs, in sharp contradiction with the observations of old and warm sources. Finally, very strong neutron or proton superfluidity ($T_{\rm c} \gtrsim 10^{10}$ K) everywhere throughout neutron star cores would suppress the direct Urca pro-
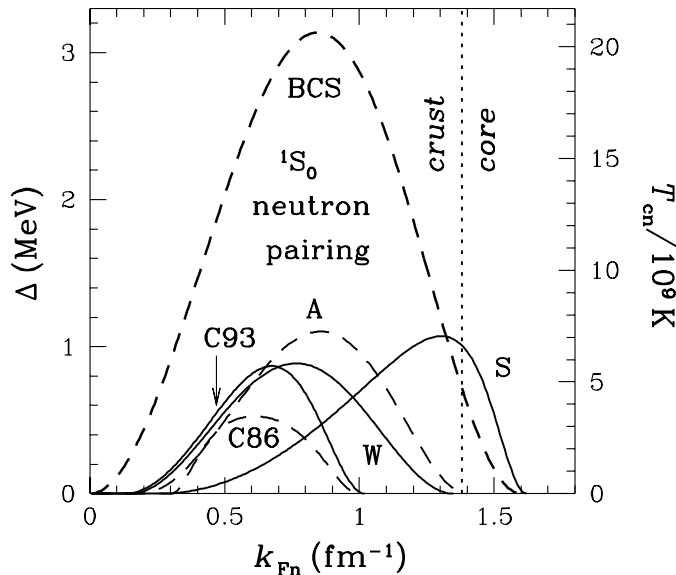
Figure 9: Energy gaps (left vertical axis) and critical temperatures (right vertical axis) for various models of crustal neutron pairing (see text) as a function of neutron Fermi wave number. The vertical dotted line marks the crust-core interface.

cess and produce slow cooling of neutron stars of any mass during the neutrino cooling stage (Yakovlev et al. 1999). This too is in conflict with observation.

5.6   Very Slowly Cooling Low-Mass Neutron Stars and the Physics of the Crust

As discussed in Sect. 5.4, low-mass stars with strong proton superfluidity in their cores form a special class of *very slowly cooling neutron stars*. Their cooling is *insensitive to the physics of the core*: to the equation of state, the stellar mass, and to the model for proton superfluidity. These stars differ from others by their very low neutrino luminosity. As a result, their cooling is *especially sensitive to the physics of the stellar crust*, since it is determined mainly by the presence of (*i*) singlet-state neutron superfluidity in the inner crust, as well as by the presence of (*ii*) accreted matter and (*iii*) magnetic fields in the blanketing envelopes. All these effects are of comparable strength. They are analyzed below following Potekhin et al. (2003) with regard to the observations of RX J0822–4300 and PSR B1055–52.

Our analysis is illustrated in Figs. 9 and 10. For definiteness, we take a 1.3 $M_\odot$ neutron star with proton superfluidity (model 1p) in the core and neglect triplet-state neutron pairing in the core (as discussed in Sect. 5.5). The two dot-dashed curves labeled *noSF* and *pSF* in each panel of Fig. 10 show the cooling of a nonsuperfluid star and a one with strong proton superfluidity, both of them without magnetic fields and accreted envelopes. As shown in Sect. 5.4, proton superfluidity delays the cooling, making it consistent with the observations of RX J0822–4300 and PSR B1055–52.
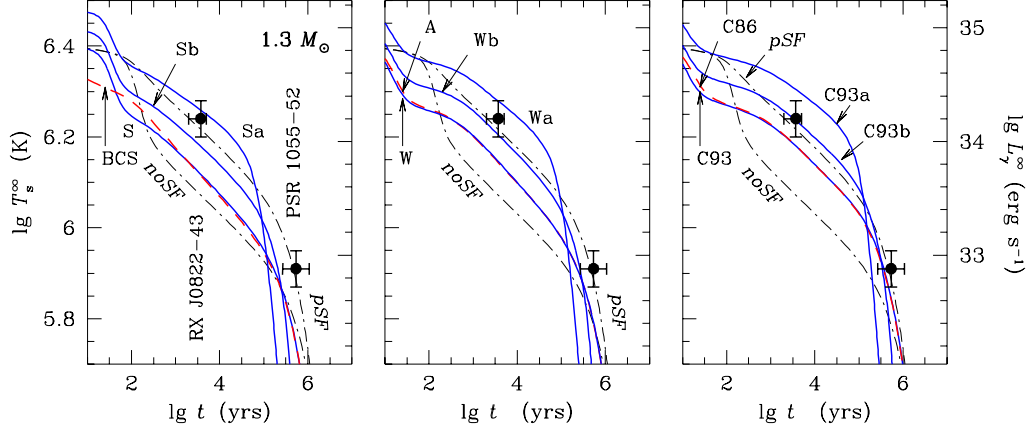
Figure 10: Evolution of redshifted effective surface temperature T_s^∞ (left-hand scale) and photon luminosity L_γ^∞ (right-hand scale) of a low-mass ($1.3\,M_\odot$) neutron star confronted with observations of RX J0822–4300 and PSR B1055–52. Dot-dashed curves: model without any superfluidity (*noSF*) or with only strong proton superfluidity (model 1p) in the core (*pSF*). Other curves include the effects of proton superfluidity in the core and a model of crustal neutron pairing from Fig. 9 (BCS or S: *left panel*; W or A: *center panel*; C86 or C93: *right panel*). Models Sa, Wa, and C93a include also the effects of fully accreted envelopes ($\Delta M/M = 10^{-7}$). Models Sb, Wb, and C93b have nonaccreted envelopes and a dipolar magnetic field $B_p = 10^{15}$ G.

The curves demonstrate how neutron superfluidity in the crust initiates neutrino emission due to the Cooper pairing of neutrons and noticeably accelerates the cooling of low-mass neutron stars (Yakovlev et al. 2001b).

For example, Fig. 9 shows the dependence of the superfluid gap Δ (left vertical axis) and the associated critical temperature T_{cn} (in units of 10^9 K, right axis) on neutron Fermi wave number k_{Fn} (as a measure of density) for six models of crustal superfluidity (from Lombardo & Schulze 2001). Model BCS is the simplest model, in which the pairing interaction it taken to be the neutron-neutron interaction in free space. The five other models – C86 (Chen et al. 1986), C93 (Chen et al. 1993), A (Ainsworth et al. 1989), W (Wambach et al. 1993), and S (Schulze et al. 1996) – include medium polarization effects which weaken the pairing. While all curves exhibit the same qualitative behavior, there are quantitatively important differences. Model BCS is oversimplified, since it does not take into account effects of the medium. In a medium, the gap is affected mainly by exchange of spin fluctuations, which reduce the gap, just as they do in metals. Model S includes the effects of spin fluctuations, and the reason for it giving results so different from the others is unclear. Despite the superficial similarity between the results of the other models, there is a spread of a factor two in the predictions for the upper density at which neutron superfluidity disappears.

Six cooling curves (BCS, S, A, W, C86, and C93) in Fig. 10 are calculated adopting the 1p model for proton superfluidity in the core and one of the models for neutron superfluidity in the crust. Crustal superfluidity accelerates the cooling and complicates the interpretation of the observations of RX J0822–4300 and PSR

B1055–52. The six curves are naturally divided into three pairs shown in three panels of Fig. 10. The curves within each pair are very close, while the pairs differ from one another. The superfluid gaps for any pair are different but disappear at the same density (Fig. 9). This density restricts the volume in which neutrino emission due to the singlet-state neutron pairing may operate and accelerate the cooling. For models BCS and S, superfluidity penetrates into the stellar core, for models A and W it dies out at the crust-core interface, while for models C86 and C93 it dies out well before the interface. Naturally, the effects of superfluidity are weakest for models C86 and C93, while models BCS and S, which are less realistic from a microscopic point of view, produce the most dramatic effect: the cooling curves lie much lower than the *pSF* curve, and are marginally inconsistent with the data.

All neutron stars are expected to have the same superfluid properties but may have different magnetic fields and envelopes. Figure 10 shows several cooling curves, where the presence of magnetic fields ($B_{\rm p} = 10^{15}$ G) or accreted envelopes ($\Delta M/M = 10^{-7}$) is taken into account in addition to the crustal superfluidity. As discussed in Sect. 5.3, magnetic fields and accreted envelopes have opposite effects on $T_{\rm s}^{\infty}$ during the neutrino and photon cooling stages. PSR B1055–52 is just passing from one cooling stage to the other and has no superstrong magnetic field. It is not expected to possess an extended accreted envelope. Thus, the effects of magnetic fields and accreted envelopes on the evolution of this pulsar are thought to be minor, but they may be important for RX J0822–4300. Including these effects, one can substantially raise the cooling curve, thereby bringing it into agreement with observation.

These results are preliminary. First, the observational data are not too certain (Sect. 2). Second, the magnetic fields and accreted envelopes have been considered as fixed. In fact, the magnetic field strength and geometry may evolve (particularly, due to ohmic decay) and the composition of surface layers may change (e.g., due to diffusive nuclear burning, Chang & Bildsten 2003). An important topic for future research is the self-consistent simulation of the magnetic, chemical, and thermal evolution of neutron stars.

As seen from Fig. 10, one can easily build a model of a middle-aged ($t \lesssim 10^4$ yr) low-mass cooling star which would be noticeably hotter than RX J0822–4300. It is sufficient to assume strong proton superfluidity in the core, crustal superfluidity according to model C86 or C93, and a massive accreted envelope. This will give a cooling curve similar to curve C93a in the right panel of Fig. 10. One can additionally push this cooling curve up by assuming a very strong magnetic field, $B_{\rm p} \gtrsim 10^{15}$ G, but this rise will be small. Thus, the C93a curve is close to the *limiting cooling curve* for the *hottest* neutron star of age $t \lesssim 10^4$ yrs. Notice that such a star will cool very quickly during the photon cooling stage.

5.7 Cooling of Old Neutron Stars. Reheating Mechanisms

Let us outline the cooling of old neutron stars ($t \gtrsim 10^5 - 10^6$ yrs, the photon cooling stage). The problem is complicated. Its important ingredient is the $T_{\rm s}-T_{\rm b}$ relation. In old stars the heat-insulating surface layer becomes extremely thin. The internal temperature is expected to become close to the surface one (very roughly) at $T_{\rm s} \lesssim 10^3$ K. Such a cold surface may be solid; its thermal emission

may be reduced by the limited transparency of surface material.

For a nonsuperfluid star without a magnetic field and without an accreted envelope, a temperature $T_s \sim 10^3$ K is reached at $t \sim 2 \times 10^7$ yrs independently of stellar mass and the presence of the enhanced neutrino emission. By that time the neutrino emission properties (crucial for $t \lesssim 10^5$ yrs) will be unimportant, and the slow and rapid cooling curves will converge to a single curve. Assuming black-body emission with $T_s \approx T_b$ during the later cooling stages, from Eq. (5) one finds the approximate cooling law $t \sim 10$ yr$/T_{s6}^2$, which gives $T_s \sim 100$ K at $t = 10^9$ yrs. The cooling of old stars is affected by superfluidity in the stellar core: strong superfluidity of nucleons suppresses the heat capacity and accelerates the cooling. For instance, strong superfluidity of neutrons and protons reduces $T_s(t)$ at $t \gtrsim 10^7$ yrs by a factor of ~ 4.

These cooling scenarios are idealized. Old neutron stars have a low heat capacity and therefore any weak reheating may drastically raise their temperatures. One such mechanism for reheating is *viscous dissipation of rotational energy* within the star. Studies of this effect were initiated by Alpar et al. (1987) and Shibazaki & Lamb (1989) who took into account viscous dissipation due to the interaction of superfluid and normal components of matter in the inner crust. The cooling theory with viscous reheating has been developed further in a number of articles cited by Page (1998a, b) and Yakovlev et al. (1999).

Reheating may also be produced by the energy release due to *weak deviations from beta equilibrium* in a neutron star core (Reisenegger 1995).

Another possibility is that a star may be heated by *ohmic dissipation of the magnetic field* in a nonsuperfluid core due to the enhancement of the electrical resistivity across a strong magnetic field. This mechanism was suggested by Haensel et al. (1990), and other references may be found in Yakovlev et al. (1999). *Ohmic decay of the magnetic field in the crust* can also heat the star (Miralles et al. 1998, Urpin & Konenkov 1998).

Reheating of old isolated neutron stars may also be provided by accretion from the interstellar medium or by pulsar activity.

As a rule, reheating mechanisms are model dependent and can produce noticeable effects only in old stars. Unfortunately, no reliable observational data on the thermal states of such stars are yet available. No reheating is required to interpret the observations of middle-aged neutron stars (Sect. 2).

6 COOLING OF NEUTRON STARS WITH EXOTIC CORES

As the next step, following Yakovlev & Haensel (2003), we explore the hypothesis of exotic matter in the cores of neutron stars. We adopt the model of neutrino emission given by Eq. (2) and shown in the left panel of Fig. 11. Quite generally, we assume the presence of an outer core with slow neutrino emission, an inner core with fast neutrino emission, and an intermediate zone ($\rho_s \lesssim \rho \lesssim \rho_f$). Using this model we obtain three types of cooling neutron stars similar to those discussed (Sect. 5.4) for stars with nucleon cores: low-mass stars ($\rho_c \lesssim \rho_s$) which cool slowly, high-mass stars ($\rho_c \gtrsim \rho_f$), which cool rapidly via enhanced neutrino emission from the inner core, and medium-mass stars ($\rho_s \lesssim \rho_c \lesssim \rho_f$), whose cooling is
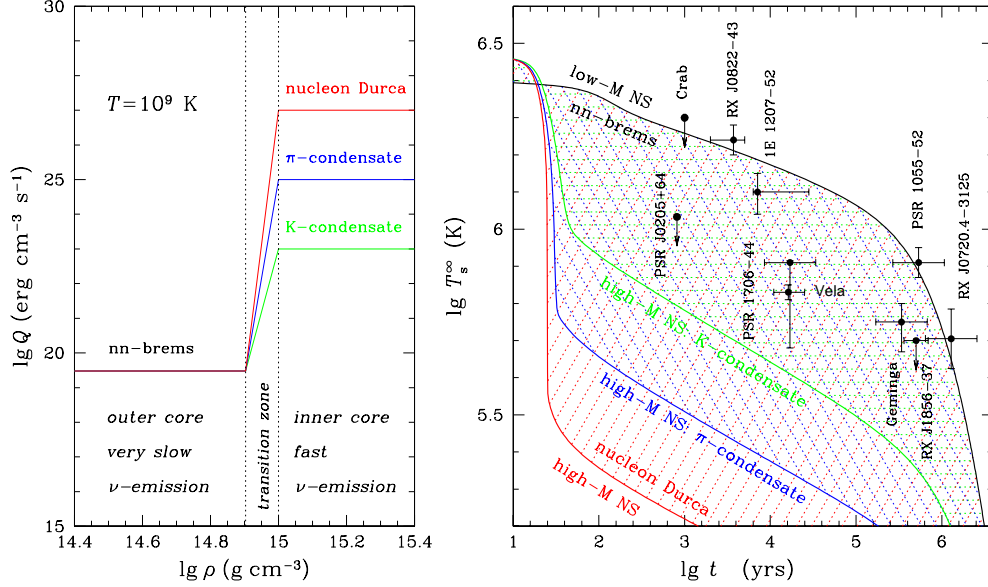
Figure 11: *Left:* Schematic model for the density dependence of the neutrino emissivity in a neutron star core at $T = 10^9$ K assuming very slow neutrino emission in the outer core and three scenarios for fast emission in the inner core. *Right:* Ranges of T_s^∞ (single, double and triple hatching) for the three types of fast emission, compared with observations. Each range is limited by the upper cooling curve which is for a low-mass star and a lower curve, which is for a high-mass star. (See text.)

intermediate.

The right panel of Fig. 11 displays cooling curves for models of low-mass and high-mass stars (no magnetic fields and accreted envelopes) for three qualitatively different equations of state and compositions for the cores, which lead to vastly different neutrino emission rates in the inner cores. We stress that the actual composition and equation of state of matter should be the same for all neutron stars, provided there is sufficient time for the matter to come into equilibrium, but at present they are unknown.

The upper cooling curve is for a low-mass star. Such neutron stars are thought to consist of nucleon matter; the cooling curves for all three equations of state have to be nearly the same. For definiteness, we present the cooling curve for a 1.35 $M_\odot$ star with strongly superfluid protons from the left panel of Fig. 6. In this case, the main neutrino emission is produced by neutron-neutron bremsstrahlung in the core.

The three lower cooling curves in the right panel of Fig. 11 refer to high-mass neutron stars with different equations of state. The lowest curve corresponds to nucleon matter. For example, we present the curve from Fig. 6 for the maximum-mass neutron star. A similar curve should describe the cooling of massive neutron stars with hyperonic cores. Two higher curves in Fig. 11 schematically show the cooling of massive neutron stars with a pion or kaon condensate in the core (with $Q_f = 10^{25}$ or 10^{23} erg cm^{-3} s^{-1} in Eq. (2), respectively). Neutron stars with

quark cores are expected to show nearly the same cooling behavior as stars with kaon condensates.

For a given equation of state for dense matter, the highest cooling curve corresponds to a low-mass star and the lowest cooling curve to a high-mass star. Between these two curves lies a sequence of cooling curves for neutron stars with masses between the highest and lowest ones (hatched regions). The data are consistent with any of the models for neutrino emission (nucleon direct Urca, pion condensate or kaon condensate), as many authors have concluded, e.g., Page, 1998a, b). Obviously, the discovery of cooler neutron stars would have important implications for the composition of matter at supernuclear densities.

The rather uniform scatter of the observational points suggests the existence of a class of intermediate mass neutron stars. Their mass range is sensitive (Yakovlev & Haensel 2003) to the position and width of the transition layer (Fig. 11) between the slow and fast neutrino emission zones. Unfortunately, these parameters cannot be constrained by the current data. For instance, ρ_s can be placed anywhere between $\sim 8 \times 10^{14}$ to $\sim 1.2 \times 10^{15}$ g cm^{-3} for a broad range of equations of state. The deduced masses of medium-mass stars will be different, but it will still be possible to explain all the sources. For kaon-condensed matter, the difference in rates between slow and fast neutrino emission processes is not too large and, consequently, stars with a significant range of stellar masses exhibit cooling behavior intermediate between the two limiting cases even if the transition zone is absent ($\rho_f = \rho_s$). In other cases the transition zone must be rather wide ($\rho_f - \rho_s \gtrsim 0.1\rho_s$) to explain the medium-mass sources. In the scenarios described in Sect. 5.4 the nonzero width of the transition zone has been produced by the weakening of proton superfluidity at high ρ.

Our analysis is a restricted one, but it has pointed to a number of general features. We have not described in detail the cooling of neutron stars with quark cores, which is very rich in physics; a comprehensive study has been carried out by Schaab et al. (1996). Nor have we considered the cooling of bare strange stars. The physics of emission from the surface of these objects is very different from that of ordinary neutron stars because of the very high plasma frequency of surface quark layers. The issue has recently been addressed by Page & Usov (2002).

7 THERMAL STATES OF TRANSIENTLY ACCRETING NEUTRON STARS

Now we discuss thermal states of accreting neutron stars in soft X-ray transients (SXRTs). We shall follow mainly the considerations of Yakovlev et al. (2003, 2004b). SXRTs undergo periods of outburst activity (lasting from days to months) superimposed on quiescent periods (lasting from months to decades); see, e.g., Chen et al. (1997). Their activity is most probably regulated by accretion from a disk around the neutron star. During quiescence, when accretion is absent or greatly suppressed, some sources emit rather intense thermal radiation, which indicates that the neutron stars are rather hot. A possible explanation for these sources (Brown et al. 1998) is that they are neutron stars powered by *deep crustal heating* (Haensel & Zdunik 1990, 2003) produced by nuclear transforma-
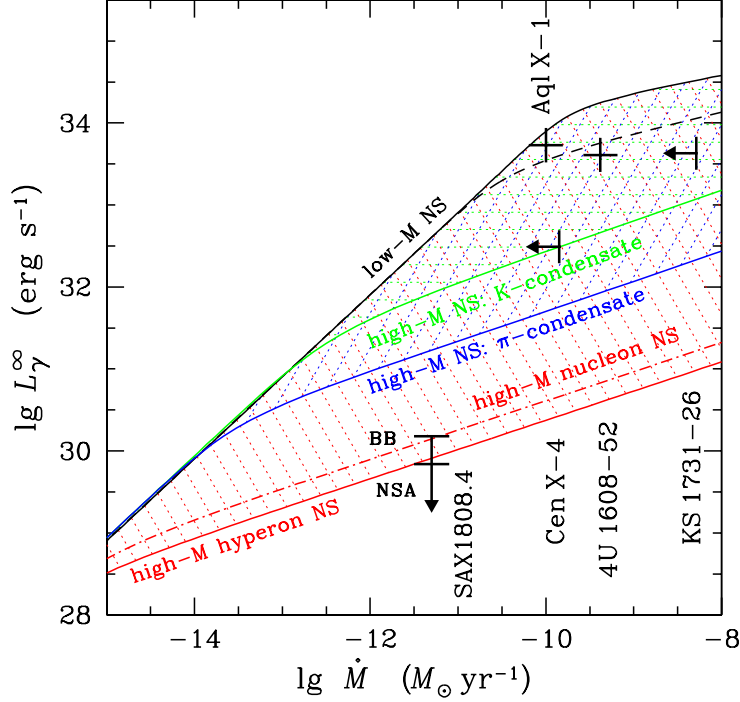
Figure 12: Quiescent thermal luminosity of several neutron stars in SXRTs versus mass accretion rate compared with theoretical curves. Three ranges of L_γ^∞ (single, double and triple hatching) correspond to the three types of fast neutrino emission. Each range is limited by the upper heating curve of a low-mass star and a lower curve of a high-mass star. See the text for details.

tions in accreted matter as it sinks into the inner crust under the weight of newly accreted material. The total energy release is about 1.1–1.5 MeV per accreted baryon, and the total heating power is $L_{\rm h} \approx (6.6-9.0) \times 10^{33} \, \dot{M}/(10^{-10} \, M_\odot \, {\rm yr}^{-1})$ erg s^{-1}, where $\dot{M}$ is the mass accretion rate. The main energy release is produced by pycnonuclear reactions at $\rho \sim (10^{12}-10^{13}) \, {\rm g \, cm}^{-3}$ (several hundred meters below the surface). The heat is spread over the neutron star by thermal conduction and radiated away by emission of photons from the surface and neutrinos from the interior. Generally, the *surface temperature depends on the internal structure of the star*, and this gives a new method for studying the internal structure.

Neutron stars in SXRTs are thermally inertial objects with thermal relaxation times $\sim 10^4$ yr (Colpi et al. 2001). Thus their internal temperatures T_i (and hence their surface temperatures) are insensitive to the transient nature of the accretion rate. Accordingly, T_i can be determined by solving the thermal balance equation (5) in the steady-state approximation: $L_{\rm h}^\infty(\dot{M}) = L_\nu^\infty(T_i) + L_\gamma^\infty$, where $\dot{M} \equiv \langle \dot{M} \rangle$ is the time-averaged accretion rate and L_γ^∞ is the quiescent thermal luminosity. A solution gives a *heating curve* – a relationship between the thermal luminosity $L_\gamma^\infty(\dot{M})$ as a function of accretion rate, or, equivalently, $T_{\rm s}^\infty(\dot{M})$. The heating curves of accreting neutron stars are closely related to the cooling curves of isolated neutron stars (e.g., Colpi et al. 2001, Yakovlev et al. 2003) since they are determined by essentially the same physics. The main difference is that the

steady states of accreting neutron stars are independent of the heat capacity of the star, although the approach to such a state does depend on the heat capacity.

By analogy with the cooling theory, accreting neutron stars may operate in the photon-emission regime ($L_\nu \ll L_\gamma \approx L_h$) or the neutrino-emission regime ($L_\nu \approx L_h \gg L_\gamma$). The latter regime, which is very sensitive to neutron star structure, is realized at higher $\dot{M}$ (e.g., Yakovlev et al. 2003). For instance, a low-mass nonsuperfluid neutron star with a core of neutrons, protons and electrons enters the neutrino-emission regime for $\dot{M} \gtrsim 3 \times 10^{-12}\ M_\odot\ yr^{-1}$, while a high-mass star does so for $\dot{M} \gtrsim 10^{-15}\ M_\odot\ yr^{-1}$.

Just as in the case of cooling isolated neutron stars (Sects. 5.4 and 6), there are three types of accreting neutron stars in the neutrino-emission regime. *Low-mass* stars have exceptionally low neutrino emission; they are the hottest for the same $\dot{M}$. *High-mass* stars have much stronger neutrino emission and are the coldest ones. *Medium-mass* stars are intermediate between the hottest and the coldest ones. The $L_\gamma^\infty(\dot{M})$ curves are sensitive to the presence in the surface layers of accreted matter containing light elements which remain unburnt in thermonuclear reactions by the beginning of a quiescent stage.

Figure 12 presents the limiting $L_\gamma^\infty(\dot{M})$ curves for three different scenarios of neutrino emission, basically the same as those studied in Sect. 6 (left panel of Fig. 11). It is assumed that thermonuclear burning in the surface layers produces Fe-like elements beneath the unburnt matter. The dashed curve is calculated for the 1.1 $M_\odot$ neutron star whose core is composed of neutrons, protons and electrons (the same equation of state as in Sect. 5) with the strong proton superfluidity model 1p. Actually, this curve is fairly insensitive to the equation of state in the core, the neutron star mass (as long as $\rho_c < \rho_s$), and the strong proton superfluidity model (just as for cooling neutron stars, Sect. 5.4). Thus, such curves obey the *universality* rule, mentioned in Sect. 5.2. For accreting neutron stars, the heating curves are more universal when plotted in terms of $L_\gamma^\infty(\dot{M})$ rather than $T_s^\infty(\dot{M})$ (Yakovlev et al. 2004b). The uppermost solid curve in Fig. 12 is the same as the dashed one but assumes the presence of $\Delta M = 10^{-8}\ M_\odot$ of light elements on the surface. Light elements make the plasma a better conductor of heat (Sect. 4.2) and thereby increase L_γ^∞ for a given $\dot{M}$.

The dot-dashed curve refers to the maximum-mass (1.977 $M_\odot$) neutron star with the same equation of state and no accreted envelope. This is the coolest accreting state for a given equation of state. The even lower, solid curve refers to the maximum-mass (1.975 $M_\odot$) neutron star with a hyperonic core (model 3 of Glendenning 1985 for the equation of state). In this case additional hyperonic direct Urca processes are allowed. They increase the neutrino emission and make the star even colder, closer to the *limit of the coldest neutron stars with nucleon-hyperon cores*. The singly hatched area in Fig. 12 is the region filled by heating curves of neutron stars of various masses ($M \gtrsim M_\odot$). It can be explained by the models of transiently accreting neutron stars with nucleon-hyperon cores. All the $L_\gamma^\infty(\dot{M})$ curves described above are taken from Yakovlev et al. (2004b).

The second and third lowest solid curves are schematic models (Yakovlev et al. 2003) for high-mass neutron stars without accreted envelopes but with pion-condensed or kaon-condensed cores, respectively (with $Q_f = 10^{25}$ or $10^{23}\ erg\ cm^{-3}\ s^{-1}$, as in Sect. 6). The third curve is about the same as for high-mass neutron

stars with quark-matter cores. Accordingly, the double and triple hatched regions can be explained by models of accreting neutron stars with pion-condensed and kaon-condensed (or quark-matter) cores.

These results are compared with observations of five SXRTs. The data are the same as those taken by Yakovlev et al. (2003, 2004b). We regard L_γ^∞ as the thermal quiescent luminosity of SXRTs, and take the values of L_γ^∞ for Aql X–1, Cen X–4, 4U 1608–552, KS 1731–26, and SAX 1808.4–3654 from Rutledge et al. (2002, 2001, 1999), Wijnands et al. (2002), and Campana et al. (2002), respectively. All these values (except that for SAX 1808.4–3654) have been obtained with the aid of hydrogen atmosphere models. The values of $\dot{M}$ for KS 1731–26 and Cen X–4 are most probably upper limits. Quiescent thermal emission has not been detected from SAX J1808.4–3658 and it is probably obscured by a rather strong non-thermal emission. We present the established upper limits of L_γ^∞ obtained by Campana et al. (2002) from the observation on March 24, 2001 (when the source was in a very low state), using either the black-body (BB) or neutron star hydrogen atmosphere (NSA) models. Since all the data are rather uncertain we plot them as large crosses or bars.

As seen from Fig. 12, we may interpret the neutron stars in 4U 1608–52 and Aql X–1 as low-mass stars with superfluid cores. These stars may be between the neutrino- and photon-emission regimes, while other neutron stars are in the neutrino-emission regime. The data on Aql X–1 are in better agreement with the models of stars with light-element envelopes (see Yakovlev et al. 2004b for details). The neutron stars in Cen X–4 and SAX J1808.4–3658 seem to require the fast neutrino cooling and thus are more massive. The status of the neutron star in KS 1731–26 is less certain because of the poorly determined $\dot{M}$; it too may require fast neutrino emission. Similar conclusions with respect to some of these sources have been arrived at by a number of authors (cited in Yakovlev et al., 2003).

The observational point for Cen X–4 lies above (or near) all three limiting curves for massive stars. Thus, we can consider the neutron star in Cen X–4 either as a high-mass star (with a kaon-condensed or quark-matter core) or as a medium-mass star (with a pion-condensed, or nucleon-hyperon core). We shall be able to explain all the data (except those for the SAX source) on the basis of any one of the three assumptions on the internal structure (exactly as for cooling neutron stars in Sect. 6).

By contrast, the data on SAX J1808.4–3658 indicate that the source contains *a very cold neutron star*. Within the framework of our interpretation, it can be explained *only as a high-mass neutron star with a nucleon or nucleon-hyperon core* (and the nucleon-hyperon core is preferable; see Yakovlev et al. 2004b, for details). However, this conclusion is based on one observation of one source and has to be confirmed in the future. Moreover, the assumption that deep crustal burning of accreted matter powers the quiescent thermal emission of SXRTs remains a hypothesis. For instance, it seems that a long-term variability of some X-ray transients in quiescent states (e.g., Aql X–1 or MXB 1659–29, see Rutledge et al. 2002 or Wijnands et al. 2004) cannot be associated with deep crustal heating. Nevertheless, deep crustal heating is a well established process (Haensel & Zdunik 1990, 2003) which is inevitable in accreting neutron stars and it must be taken

into account.

8 CONCLUSIONS

As a consequence of improved measurements of thermal emission from cooling neutron stars in recent years, it has become very clear that the observations cannot be explained on the basis of a single universal cooling curve. If thermal radiation from neutron stars in soft X-ray transient sources is due to nuclear burning processes deep in the crust, the observations of isolated neutron stars and X-ray transients can be analyzed within a common theoretical framework. Moreover, observations may be explained in terms of physically reasonable models.

The basic ingredients of such a model are:

(a) In the cores of massive neutron stars, a neutrino emission process faster than the modified Urca one operates. If one disregards the observations of SAX J1808.4–3658, it is not possible to pin down which of the faster processes (direct Urca processes for nucleons and hyperons, a pion condensate, a kaon condensate, or quark matter) is responsible, but if one includes the data from SAX J1808.4–3658, the nucleon or hyperon direct Urca process would be favored, and the other possibilities would be excluded.

(b) In the cores of low-mass stars, neutrino emission is slower than that produced by the modified Urca process. For instance, this emission may be provided by neutron-neutron bremsstrahlung while other potentially efficient neutrino processes may be suppressed by strong superfluidity of protons.

(c) Medium-mass stars show cooling intermediate between slow and fast. In particular, they may cool via enhanced neutrino emission partly suppressed by proton superfluidity. The mass range for these stars is determined by the density range over which the transition in the neutrino emission rate from slow to fast occurs. Some physical models of neutron star interiors contradict observations, for instance, the model of mild $^3P_2$ neutron superfluidity in the stellar cores with a maximum superfluid transition temperature $T_{cn}(\rho)$ in the range from 2×10^8 to 2×10^9 K.

It is unlikely that advances in understanding the nature of the interiors of neutron stars will come from a single piece of evidence, but rather from a systematic appraisal of a variety of different sorts of evidence, just as in many legal cases. Directions for future study include:

• Further observations of thermal radiation from neutron stars. A search for new very cold or very hot stars would be useful. Very cold neutron stars would rule out the possibility of not too fast neutrino emission produced by exotic matter in neutron star cores.

• Further theoretical investigations of the effects of correlations in dense matter. In particular, the role of tensor correlations needs to be reexamined following the work of Akmal & Pandharipande (1997), which found a strong increase of tensor correlations, a sign of incipient pion condensation at relatively low densities, and the recent study by Schwenk & Friman (2004) which pointed to the strong modification of the tensor force by the nuclear medium.

• Information about neutron stars obtained from studies of cooling needs to be integrated with what has been learned by other means. Examples are

other observations of neutron stars, for instance, measurements of their radii or gravitational redshifts. Of special importance are observations of neutron stars in binary systems, which can be used to determine neutron star masses. Even a firm lower bound on a neutron star mass obtained from, e.g., radio observations of compact binaries containing pulsars (either binary neutron stars or pulsar–white-dwarf binaries, such as J0751+1807 reported recently by Nice et al. 2004), could rule out a number of theoretical equations of state. It is also important to ensure that the physical input to neutron star calculations is consistent with experimental nuclear physics data on correlations between nucleons, hyperons and other degrees of freedom in dense matter.

References

Ainsworth TL, Wambach J, Pines D. 1989. Effective interactions and superfluid energy gaps for low density neutron matter. *Phys. Lett.* B222:173–78

Akmal A, Pandharipande VR. 1997. Spin-isospin structure and pion condensation in nucleon matter. *Phys. Rev.* C56:2261–79

Alford M. 2004. Dense quark matter in Nature. In *Finite Density QCD at Nara*. In press [nucl-th/0312007]

Alford M, Rajagopal K, Wilczek F. 1998. QCD at finite baryon density: nucleon droplets and color superconductivity. *Phys. Lett.* B422:247–56

Alpar A, Brinkmann W, Ögelman H, Kiziloğlu Ü, Pines D. 1987. A search for X-ray emission from a nearby pulsar – PSR 1929+10. *Astron. Astrophys.* 177:101–04

Arendt RG, Dwek E, Petre R. 1991. An infrared analysis of Puppis A. *Astrophys. J.* 368:474–85

Baiko DA, Yakovlev DG. 1999. Direct Urca process in strong magnetic fields and neutron star cooling. *Astron. Astrophys.* 342:192–200

Bailin D, Love A. 1984. Superfluidity and superconductivity in relativistic fermion systems. *Phys. Rep.* 107:325–85

Balberg S, Barnea N. 1998. S-wave pairing of Lambda hyperons in dense matter. *Phys. Rev.* C57:409–16

Baym G, Campbell DK. 1978. Chiral symmetry and pion condensation. In *Mesons in Nuclei*, ed. M Rho, D Wilkinson, Vol. III, pp. 1031–1094. Amsterdam: North-Holland

Baym G, Pethick C, Pines D. 1969. Superfluidity in neutron stars. *Nature* 224:673–74

Braje TM, Romani RW. 2002. RX J1856-3754: Evidence for a stiff equation of state. *Astrophys. J.* 580:1043–47

Brisken WF, Thorsett SE, Golden A, Goss WM. 2003. The distance and radius of the neutron star PSR B0656+14. *Astrophys. J.* 593:L89–92

Brown GE. 1995. Kaon condensation in dense matter. In: *Bose–Einstein Condensation*, ed. A Griffin, DW Snoke, S Stringari, pp. 438–51. Cambridge: Cambridge Univ. Press

Brown EF, Bildsten L, Rutledge RE. 1998. Crustal heating and quiescent emission from transiently accreting neutron stars. *Astrophys. J.* 504:L95–98

Burwitz V, Haberl F, Neuhäuser R, Predehl P, Trümper J, Zavlin VE. 2003. The thermal radiation of the isolated neutron star RX J1856.5-3754 observed with Chandra and XMM-Newton. *Astron. Astrophys.* 399:1109–14

Campana S, Stella L, Gastaldello F, Mereghetti S, Colpi M, Israel GL, Burderi L, Di Salvo T, Robba RN. 2002. An XMM-Newton study of the 401 Hz accreting pulsar SAX J1808.4–3658 in quiescence. *Astrophys. J.* 575:L15–19

Caraveo PA, Bignami GF, Mignani R, Taff LG. 1996. Parallax observations with the Hubble Space Telescope yield the distance to Geminga. *Astrophys. J.* 461:L91–94

Caraveo PA, De Luca A, Mignani RP, Bignami GF. 2001. The distance to the Vela pulsar gauged with Hubble Space Telescope parallax observations. *Astrophys. J.* 561:930–37

Carter GW, Prakash M. 2002. The quenching of the axial coupling in nuclear and neutron-star matter. *Phys. Lett.* B525:249–54

Chang P, Bildsten L. 2003. Diffusive nuclear burning in neutron star envelopes. *Astrophys. J.* 585:464–74

Chen JMC, Clark JW, Krotscheck E, Smith RA. 1986. Nucleonic superfluidity in neutron stars: $^1S_0$ neutron pairing in the inner crust. *Nucl. Phys.* A451:509–40

Chen JMC, Clark JW, Davé RD, Khodel VV. 1993. Pairing gaps in nucleonic superfluids. *Nucl. Phys.* A555:59–89

Chen W, Shrader CR, Livio M. 1997. The properties of X-ray and optical light curves of X-ray novae. *Astrophys. J.* 491:312–38

Colpi M, Geppert U, Page D, Possenti A. 2001. Charting the temperature of the hot neutron star in a soft X-ray transient. *Astrophys. J.* 548:L175–78

Dodson D, Legge D, Reynolds JE, McCulloch PM. 2003. The Vela Pulsar's proper motion and parallax derived from VLBI observations. *Astrophys. J.* 596:1137–41

Flowers EG, Ruderman M, Sutherland PG. 1976. Neutrino pair emission from finite-temperature neutron superfluid and the cooling of young neutron stars. *Astrophys. J.* 205:541–44

Gamow G, Schoenberg M. 1941. Neutrino theory of stellar collapse. *Phys. Rev.* 59:539–47

Gnedin OY, Yakovlev DG, Potekhin AY. 2001. Thermal relaxation in young neutron stars. *Mon. Not. Roy. Astron. Soc.* 324:725–36

Glen G, Sutherland P. 1980. On the cooling of neutron stars. *Astrophys. J.* 239:671–84

Glendenning NK. 1985. Neutron stars are giant hypernuclei? *Astrophys. J.* 293:470–93

Glendenning N. 1996. Compact Stars. Nuclear Physics, Particle Physics and General Relativity. Springer-Verlag: New York

Gudmundsson EH, Pethick CJ, Epstein RI. 1983. Structure of neutron star envelopes. *Astrophys. J.* 272:286–300

Gusakov ME. 2002. Neutrino emission from superfluid neutron-star cores: various types of neutron pairing. *Astron. Astrophys.* 389:702–15

Haensel P. 2003. Equation of state of dense matter and maximum mass of neutron stars. In *Final Stages of Stellar Evolution*, ed. C Motch, J-M Hameury, pp. 249–84. EAS Publications Series: EDP Sciences.

Haensel P, Zdunik JL. 1990. Non-equilibrium processes in the crust of an accreting neutron star. *Astron. Astrophys.* 227:431–36

Haensel P, Zdunik JL. 2003. Nuclear composition and heating in accreting neutron-star crusts. *Astron. Astrophys.* 404:L33–36

Haensel P. Urpin VA, Yakovlev DG. 1990. Ohmic decay of internal magnetic fields in neutron stars. *Astron. Astrophys.* 229:133–37

Halpern JP, Wang FY-H. 1997. A broadband X-ray study of the Geminga pulsar. *Astrophys. J.* 477:905–15

Hanhart C, Phillips DR, Reddy S. 2001. Neutrino and axion emissivities of neutron stars from nucleon-nucleon scattering data. *Phys. Lett.* B499:9–15

Hoffberg M, Glassgold AE, Richardson RW, Ruderman M. 1970. Anisotropic superfluidity in neutron star matter. *Phys. Rev. Lett.* 24:775–77

Friman BL, Maxwell OV. 1979. Neutrino emissivities of neutron stars. *Astrophys. J.* 232:541–57

Jaikumar P, Prakash M. 2001. Neutrino pair emission from Cooper pair breaking and recombination in superfluid quark matter. *Phys. Lett.* B516:345–52

Kaminker AD, Haensel P, Yakovlev DG. 2001. Nucleon superfluidity vs. observations of cooling neutron stars. *Astron. Astrophys.* 373:L17–20

Kaminker AD, Yakovlev DG, Gnedin OY. 2002. Three types of cooling superfluid neutron stars: Theory and observations. *Astron. Astrophys.* 383:1076–87

Kaplan DB, Nelson AE. 1986. Strange goings on in dense nucleonic matter. *Phys. Lett.* B175:57–63. Erratum: 179:409

Kaplan DL, Kulkarni SR, van Kerkwijk MH, Marshall HL. 2002. X-ray timing of the enigmatic neutron star RX J0720.4-3125. *Astrophys. J.* 570:L79–L83

Lattimer JM, Prakash M. 2001. Neutron star structure and the equation of state. *Astrophys. J.* 550:426–42

Lattimer JM, Pethick CJ, Prakash M, Haensel P. 1991. Direct Urca process in neutron stars. *Phys. Rev. Lett.* 66:2701–04

Lattimer JM, van Riper KA, Prakash M, Prakash M. 1994. Rapid cooling and the structure of neutron stars. *Astrophys. J.* 425:802–13

Lombardo U, Schulze H-J. 2001. Superfluidity in neutron star matter. In *Physics of Neutron Star Interiors*, ed. D Blaschke, NK Glendenning, A Sedrakian, pp. 30–53. Springer: Berlin

Lorenz CP, Ravenhall DG, Pethick CJ. 1993. Neutron star crusts. *Phys. Rev. Lett.* 70:379–82

Lyne AG, Pritchard RS, Graham-Smith F, Camilo F. 1996. Very low braking index for the Vela pulsar. *Nature* 381:497–98

McGowan KE, Zane S, Cropper M, Kennea JA, Córdova FA, Ho C, Sasseen T, Vestrand WT. 2004. XMM-Newton observations of PSR B1706–44. *Astrophys. J.* 600:343–50

Migdal AB. 1959. Superfluidity and the moments of inertia of nuclei. *Nucl. Phys.* 13:655–74

Migdal AB. 1971. Stability of vacuum and limiting fields. *Uspekhi Fiz. Nauk* 105:781–81

Miralles JA, Urpin VA, Konenkov DYu. 1998. Joule heating and the thermal evolution of old neutron stars. *Astrophys. J.* 503:368–73

Motch C, Zavlin VE, Haberl F. 2003. The proper motion and energy distribution of the isolated neutron star. *Astron. Astrophys.* 408:323–30

Negele JW, Vautherin D. 1973. Neutron star matter at sub-nuclear densities. *Nucl. Phys.* A207:298–320

Nice DJ, Splaver EM, Stairs IH. 2004. Heavy neutron stars? A status report on Arecibo timing of four pulsar – white dwarf systems. In *Young Neutron Stars and Their Environments*, IAU Symposium No. 218, ed. F Camilo, BM Gaensler. In press [astro-ph/0311296]

Oyamatsu K. 1993. Nuclear shapes in the inner crust of a neutron star. *Nucl. Phys.* A561:431–52

Page D. 1993. The Geminga neutron star: evidence for nuclear superfluidity at very high density. In *Proc. of the First Symposium on Nuclear Physics in the Universe*, ed. MR Strayer, MW Guidry, p. 15. Bristol: Adam Hilger

Page D. 1995. Surface temperature of a magnetized neutron star and interpretation of the ROSAT data. 1: Dipole fields. *Astrophys. J.* 442:273–85

Page D. 1998a. Thermal evolution of isolated neutron stars. In *The Many Faces of Neutron Stars*, ed. R Buccheri, J van Paradijs, MA Alpar, pp. 539–52. Kluwer: Dordrecht

Page D. 1998b. Thermal evolution of isolated neutron stars. In *Neutron Stars and Pulsars*, ed. N Shibazaki, N Kawai, S Shibata, T Kifune, pp. 183–94. Universal Academy Press: Tokyo

Page D, Applegate JH. 1992. The cooling of neutron stars by the direct Urca process. *Astrophys. J.* 394:L17–20

Page D, Usov VV. 2002. Thermal evolution and light curves of young bare strange stars. *Phys. Rev. Lett.* 89:131101

Pavlov GG. 2003. Private communication

Pavlov GG, Zavlin VE. 2003. Thermal radiation from cooling neutron stars. In *Texas in Tuscany. XXI Texas Symposium on Relativistic Astrophysics*, ed. R Bandiera, R Maiolino, F Mannucci, pp. 319–28. Singapore: World Scientific Publishing

Pavlov GG, Zavlin VE, Sanwal D, Burwitz V, Garmire GP. 2001. The X-Ray spectrum of the Vela pulsar resolved with the Chandra X-ray observatory. *Astrophys. J.* 552:L129–33

Pavlov GG, Zavlin VE, Sanwal D, Trümper J. 2002a. 1E 1207.4–5209: The puzzling pulsar at the center of the supernova remnant PKS 1209–51/52. *Astrophys. J.* 569:L95–98

Pavlov GG, Zavlin VE, Sanwal D. 2002b. Thermal radiation from neutron stars: Chandra results. In *270 WE-Heraeus Seminar on Neutron Stars, Pulsars and Supernova Remnants*, ed. W Becker, H Lesh, J Trümper, pp. 273–86. MPE: Garching

Pethick CJ. 1992. Cooling of neutron stars. *Rev. Mod. Phys.* 64:1133–40

Pethick CJ, Ravenhall DG. 1995. Matter at large neutron excess and the physics of neutron-star crusts. *Ann. Rev. Nucl. Particle Sci.* 45:429–84

Pons JA, Miralles JA, Prakash M, Lattimer JM. 2001. Evolution of proto-neutron stars with kaon condensates. *Astrophys. J.* 553:382–93

Potekhin AY, Yakovlev DG. 2001. Thermal structure and cooling of neutron stars with magnetized envelopes. *Astron. Astrophys.* 374:213–26

Potekhin AY, Chabrier G, Yakovlev DG. 1997. Internal temperatures and cooling of neutron stars with accreted envelopes. *Astron. Astrophys.* 323:415–28

Potekhin AY, Yakovlev DG, Chabrier G, Gnedin OY. 2003. Thermal structure and cooling of superfluid neutron stars with accreted magnetized envelopes. *Astrophys. J.* 594:404–18

Prakash M, Ainsworth TL, Lattimer JM. 1988. Equation of state and the maximum mass of neutron stars. *Phys. Rev. Lett.* 61:2518–21

Prakash M, Prakash M, Lattimer JM, Pethick CJ. 1992. Rapid cooling of neutron stars by hyperons and Δ-isobars. *Astrophys. J.* 390:L77–80

Rutledge RE, Bildsten L, Brown EF, Pavlov GG, Zavlin VE. 1999. The thermal X-Ray spectra of Centaurus X–4, Aquila X–1, and 4U 1608–522 in quiescence. *Astrophys. J.* 514:945–51

Rutledge RE, Bildsten L, Brown EF, Pavlov GG, Zavlin VE. 2000. A method for distinguishing between transiently accreting neutron stars and black holes, in quiescence. *Astrophys. J.* 529:985–96

Rutledge RE, Bildsten L, Brown EF, Pavlov GG, Zavlin VE. 2002. Variable thermal emission from Aquila X-1 in quiescence. *Astrophys. J.* 577:346–58

Reisenegger A. 1995. Deviation from chemical equilibrium due to spin-down as an internal heat source in neutron stars. *Astrophys. J.* 442:749–57

Sanwal D, Pavlov GG, Zavlin VE, Teter MA. 2002. Discovery of absorption features in the X-ray spectrum of an isolated neutron star. *Astrophys. J.* 574:L61–64

Sawyer RF. 1972. Condensed π^- phase of neutron star matter. *Phys. Rev. Lett.* 29:382–85

Scalapino DJ. 1972. π^- condensate in dense nuclear matter. *Phys. Rev. Lett.* 29:386–88

Schaab Ch, Weber F, Weigel MK, Glendenning NK. 1996. Thermal evolution of compact stars. *Nucl. Phys.* A605:531–65

Schulze H-J, Cugnon J, Lejeune A, Baldo M, Lombardo U. 1996. Medium polarization effects on neutron matter superfluidity. *Phys. Lett.* B375:1–8

Schwenk A., Friman B. 2004. Polarization contributions to the spin-dependence of the effective interaction in neutron matter. *Phys. Rev. Lett.* in press [nucl-th/0307089]

Schwenk A, Jaikumar P, Gale C. 2004. Neutrino bremsstrahlung in neutron matter from effective nuclear interactions. *Phys. Lett. B* in press [nucl-th/0309072]

Shapiro SL, Teukolsky SA. 1983. Black Holes, White Dwarfs, and Neutron Stars. Wiley-Interscience: New York

Shibazaki N, Lamb FK. 1989. Neutron star evolution with internal heating *Astrophys. J.* 346:808–22

Slane PO, Helfand DJ, Murray SS. 2002. New constraints on neutron star cooling from Chandra observations of 3C 58. *Astrophys. J.* 571:L45–49

Takatsuka T, Tamagaki R. 1995. Nucleon superfluidity in kaon-condensed neutron stars. *Progr. Theor. Phys.* 94:457–61

Takatsuka T., Tamagaki R. 1997. Effects of charged-pion condensation on neutron $^3P_2$ superfluidity. *Progr. Theor. Phys.* 97:263–81

Thorne KS. 1977. The relativistic equations of stellar structure and evolution. *Astrophys. J.* 212:825–31

Tsuruta S. 1998. Thermal properties and detectability of neutron stars. II. Thermal evolution of rotation-powered neutron stars. *Phys. Rep.* 292:1–130

Tsuruta S, Cameron AGW. 1966. Cooling and detectability of neutron stars. *Canad. J. Phys.* 44:1863–94

Urpin VA, Konenkov DYu. 1998. Magnetic evolution of neutron stars. In *Neutron Stars and Pulsars*, ed. N Shibazaki, N Kawai, S Shibata, T Kifune, pp. 171–78. Universal Academy Press: Tokyo

Ushomirsky G, Rutledge RE. 2001. Time-variable emission from transiently accreting neutron stars in quiescence due to deep crustal heating. *Mon. Not. Roy. Astron. Soc.* 325:1157–66

van Dalen ENE, Dieperink AEL, Tjon JA. 2003. Neutrino emission in neutron stars. *Phys. Rev.* C67:065807

Walter FM, Lattimer JM. 2002. A revised parallax and its implications for RX J185635–3754. *Astrophys. J.* 576:L145–48

Wambach J, Ainsworth TL, Pines D. 1993. Quasiparticle interactions in neutron matter for applications in neutron stars. *Nucl. Phys.* A555:128–50

Weber F. 1999. *Pulsars as Astrophysical Laboratories for Nuclear and Particle Physics.* Institute of Physics Publishing: Bristol

Weisskopf MC, O'Dell SL, Paerels F, Becker W, Tennant AF, Swartz D. 2004. Chandra phase-resolved X-ray spectroscopy of the Crab pulsar. *Astrophys. J.* In print [astro-ph/0310332]

Wijnands R, Guainazzi M, van der Klis M, Méndez M. 2002. XMM-Newton observations of the neutron star X-ray transient KS 1731–260 in quiescence. *Astrophys. J.* 573:L45–49

Wijnands R, Homan J, Miller JM, Lewin WHG. 2004. Monitoring Chandra observations of the quasi-persistent neutron-star X-ray transient MXB 1659–29 in quiescence: the cooling curve of the heated neutron-star crust. *Astrophys. J.* submitted [astro-ph/0310612]

Winkler PF, Tuttle JH, Kirshner RP, Irwin MJ. 1988. Kinematics of oxygen-rich filaments in Puppis A. In *Supernova Remnants and the Interstellar Medium*, ed. RS Roger, TL Landecker, p. 65. Cambridge: Cambridge Univ. Press

Wolf RA. 1966. Some effects of the strong interactions on the properties of neutron-star matter. *Astrophys. J.* 145:834–41

Yakovlev DG, Haensel P. 2003. What we can learn from observations of cooling neutron stars. *Astron. Astrophys.* 407:259–64

Yakovlev DG, Levenfish KP, Shibanov YuA. 1999. Cooling of neutron stars and superfluidity in their cores. *Uspekhi Fiz. Nauk* 169:825–68 (English translation: *Physics – Uspekhi* 42:737–78)

Yakovlev DG, Kaminker AD, Gnedin OY, Haensel P. 2001a. Neutrino emission from neutron stars. *Phys. Rep.* 354:1–155

Yakovlev DG, Kaminker AD, Gnedin OY. 2001b. $^1S_0$ neutron pairing vs. observations of cooling neutron stars. *Astron. Astrophys.* 379:L5–8

Yakovlev DG, Kaminker AD, Haensel P, Gnedin OY. 2002a, The cooling neutron star in 3C 58. *Astron. Astrophys.* 389:L24–27

Yakovlev DG, Gnedin OY, Kaminker AD, Potekhin AY. 2002b. Cooling of superfluid neutron stars. In *270 WE-Heraeus Seminar on Neutron Stars, Pulsars and Supernova Remnants*, ed. W Becker, H Lesh, J Trümper, pp. 287–99. MPE: Garching

Yakovlev DG, Levenfish KP, Haensel P. 2003. Thermal state of transiently accreting neutron stars. *Astron. Astrophys.* 407:265–71

Yakovlev DG, Gnedin OY, Kaminker AD, Levenfish KP, Potekhin AY. 2004a. Neutron star cooling: theoretical aspects and observational constraints. *Adv. Space Res.* In press [astro-ph/0306143]

Yakovlev DG, Levenfish KP, Potekhin AY, Gnedin OY, Chabrier G. 2004b. Thermal states of coldest and hottest neutron stars in soft X-ray transients. *Astron. & Astrophys.* In press [astro-ph/0310259]

Zavlin VE, Pavlov GG. 2002. Modeling neutron star atmospheres. In *270 WE-Heraeus Seminar on Neutron Stars, Pulsars and Supernova Remnants*, ed. W Becker, H Lesh, J Trümper, pp. 263–72. MPE: Garching

Zavlin VE, Pavlov GG. 2004. XMM observations of three middle-aged pulsars. *Memorie della Societa' Astronomica Italiana.* In press [astro-ph/0312326]

Zavlin VE, Pavlov GG, Trümper J. 1998. The neutron star in the supernova remnant PKS 1209–52. *Astron. Astrophys.* 331:821–28

Zavlin VE, Trümper J, Pavlov GG. 1999. X-ray emission from the radio-quiet neutron star in Puppis A. *Astrophys. J.* 525:959–67